JCB: Article

Inhibition of endothelial FAK activity prevents tumor metastasis by enhancing barrier function

Christine Jean,[1] Xiao Lei Chen,[1] Ju-Ock Nam,[3] Isabelle Tancioni,[1] Sean Uryu,[1] Christine Lawson,[1] Kristy K. Ward,[1] Colin T. Walsh,[4] Nichol L.G. Miller,[1] Majid Ghassemian,[5] Patric Turowski,[6] Elisabetta Dejana,[7,8] Sara Weis,[2] David A. Cheresh,[2] and David D. Schlaepfer[1]

[1]Department of Reproductive Medicine and [2]Department of Pathology, Moores University of California, San Diego Cancer Center, La Jolla, CA 92093
[3]Kyungpook National University, Gyeongsangbuk-do 742-711, Korea
[4]Bionomics, San Diego, CA 92109
[5]Department of Chemistry and Biochemistry, University of California, San Diego, La Jolla, CA 92093
[6]Department of Cell Biology, Institute of Ophthalmology, University College London, London EC1V 9EL, England, UK
[7]Italian Foundation for Cancer Research Institute of Molecular Oncology and [8]Department of Biosciences, University of Milan, 20122 Milano, Italy

Pharmacological focal adhesion kinase (FAK) inhibition prevents tumor growth and metastasis, via actions on both tumor and stromal cells. In this paper, we show that vascular endothelial cadherin (VEC) tyrosine (Y) 658 is a target of FAK in tumor-associated endothelial cells (ECs). Conditional kinase-dead FAK knockin within ECs inhibited recombinant vascular endothelial growth factor (VEGF-A) and tumor-induced VEC-Y658 phosphorylation in vivo. Adherence of VEGF-expressing tumor cells to ECs triggered FAK-dependent VEC-Y658 phosphorylation. Both FAK inhibition and VEC-Y658F mutation within ECs prevented VEGF-initiated paracellular permeability and tumor cell transmigration across EC barriers. In mice, EC FAK inhibition prevented VEGF-dependent tumor cell extravasation and melanoma dermal to lung metastasis without affecting primary tumor growth. As pharmacological c-Src or FAK inhibition prevents VEGF-stimulated c-Src and FAK translocation to EC adherens junctions, but FAK inhibition does not alter c-Src activation, our experiments identify EC FAK as a key intermediate between c-Src and the regulation of EC barrier function controlling tumor metastasis.

Introduction

Tumor spread remains a primary cause of cancer mortality (Eccles and Welch, 2007). Metastasis involves cell migration from the primary tumor site, cell intravasation into blood or lymph vessels, and extravasation at distant sites (Chiang and Massagué, 2008). Extravasation requires tumor cell adhesion to endothelial cells (ECs), breakdown of EC junctions, and tumor cell transmigration across ECs (Steeg, 2006).

EC barrier function is mediated in part by homotypic binding of transmembrane adherens junction proteins such as vascular endothelial cadherin (VEC; Dejana et al., 2009). Post-translational VEC modifications trigger junctional changes, VEC internalization, and increased vascular permeability, which can modulate tumor cell intravasation and extravasation (Dejana et al., 2008; Le Guelte et al., 2011).

VEGF, a growth factor produced by various cancers (Poon et al., 2001), is an important molecule promoting tumor–EC cross talk. VEGF-A, via the binding to a VEGF receptor (VEGFR-2) on ECs (Olsson et al., 2006), triggers rapid VEC tyrosine (Y) phosphorylation and results in VEC–β-catenin–p120-catenin–α-catenin complex dissociation (Potter et al., 2005) and increased vascular permeability. These rapid events precede angiogenesis (Claesson-Welsh and Welsh, 2013).

Different signaling pathways promote VEC phosphorylation, but this regulation remains undefined in vivo. c-Src and FAK-related Pyk2 are implicated in VEC phosphorylation at Y645, Y731, and Y733 after ICAM-1 engagement and involved in lymphocyte transmigration (Allingham et al., 2007; Turowski et al., 2008). VEGF can promote Y685 VEC phosphorylation via c-Src activation (Wallez et al., 2007), resulting in Csk binding

Correspondence to David D. Schlaepfer: dschlaepfer@ucsd.edu

Abbreviations used in this paper: CMFDA, 5-chloromethylfluorescein diacetate; EC, endothelial cell; ER(T), estrogen receptor tamoxifen; FAK-I, FAK inhibitor; H&E, hematoxylin and eosin; HPAEC, human pulmonary aortic EC; HUVEC, human umbilical vein EC; KD, kinase dead; mHLEC, mouse heart and lung EC; MS, mass spectrometry; VEC, vascular endothelial cadherin; WT, wild type.
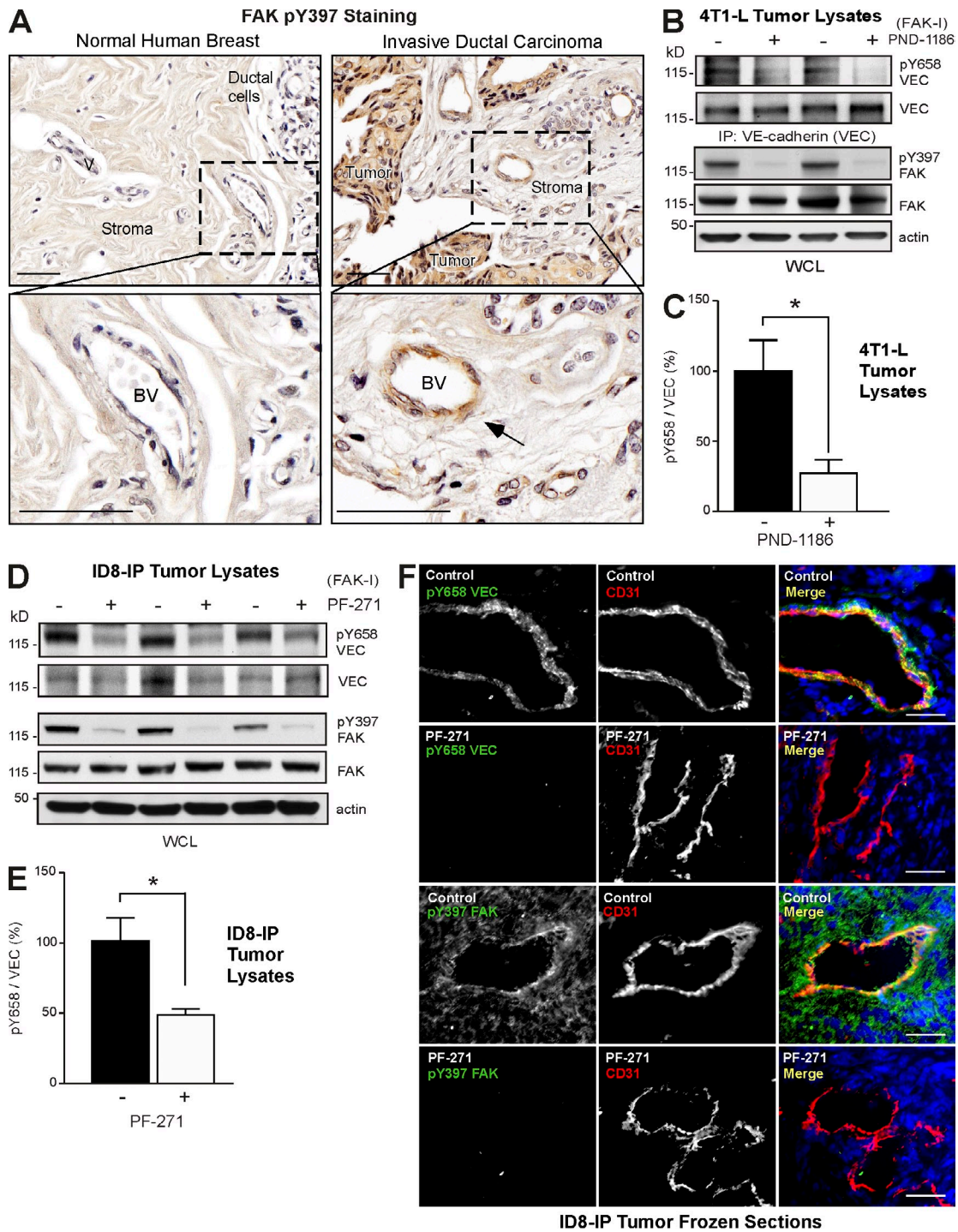
Figure 1. **Pharmacological FAK inhibition prevents tumor-associated VEC-Y658 phosphorylation.** (A) Phosphospecific antibody to FAK-Y397 (pY397, brown) staining of paraffin-embedded normal human breast and invasive ductal carcinoma samples. Sections were counterstained with hematoxylin (blue). Indicated are ductal cells, tumor, stroma, and blood vessels (BV). The boxed regions were enlarged (bottom images), and the arrow indicates a tumor–stromal blood vessel with strong pY397 FAK staining. (B) 4T1-L breast carcinoma cells were implanted in the mammary fat pad of BALB/c mice. After 48 h, mice were provided with 5% sucrose (control) or 0.5 mg/kg PND-1186 in 5% sucrose ad libitum in the drinking water. After 18 d, 4T1-L tumor protein lysates (two independent controls and two treated with PND-1186) were analyzed by VEC pY658 and FAK pY397 immunoblotting. Blots were reprobed for total VEC, FAK, and actin expression. IP, immunoprecipitation; WCL, whole-cell lysate. (C) Densitometry of VEC pY658 in 4T1-L tumors from control and PND-1186–treated mice. Values are mean percentages (pY658/total VEC) ± SEM from four independent tumors per experimental point (*, P < 0.05). The mean of vehicle-treated tumors was set to 100. (D) ID8-IP tumor cells were microinjected into the ovarian space, and after 7 d, vehicle or 30 mg/kg PF-271 was administered by oral gavage twice daily. After 28 d, ID8-IP tumor lysates (three independent controls and three treated with PF-271) were analyzed by VEC pY658 and FAK pY397 immunoblotting. Blots were reprobed for total VEC, FAK, and actin expression. (E) Densitometry of VEC pY658 in ID8-IP tumors from vehicle and PF-271–treated mice. Values are mean percentages (pY658/total VEC) ± SEM from three independent tumors per experimental point (*, P < 0.05). The mean of vehicle-treated tumors was set to 100. (F) Control or PF-271–treated ID8-IP tumors were analyzed by combined staining for ECs (CD31), VEC pY658, or activated FAK (pY397 FAK) as indicated. Merged images (DAPI nuclear stain, blue) show VEC pY658 staining in association with ECs (yellow) only in vehicle control–treated mice. Bars, 50 µm.

to VEC (Baumeister et al., 2005). VEC-Y658 phosphorylation disrupts p120-catenin binding, and this is implicated in promoting adherens junction dissolution and increased permeability (Potter et al., 2005). However, the molecular mechanisms controlling VEC-Y658 phosphorylation in tissues and tumors in response to VEGF remain unresolved.

FAK is a cytoplasmic tyrosine kinase coactivated by integrin and VEGFR-2 receptors in the control of vascular permeability (Chen et al., 2012). Small molecule FAK inhibitors (FAK-Is) prevent tumor progression in mice (Schwock et al., 2010) and are being evaluated in clinical trials (Infante et al., 2012). Targets of FAK inhibition include blocking tumor (Tanjoni et al., 2010), stromal fibroblast (Stokes et al., 2011), inflammatory (Walsh et al., 2010), or angiogenesis signaling (Tavora et al., 2010). FAK expression and activation (as measured by FAK-Y397 phosphorylation) are also elevated in ECs associated with malignant astrocytoma and ovarian tumors (Haskell et al., 2003; Lu et al., 2007). Genetic inactivation of FAK activity results in embryonically lethal vascular defects (Lim et al., 2010, 2012; Zhao et al., 2010). However, conditional kinase-dead (KD) FAK knockin within adult mouse ECs bypasses lethality and revealed an important role for FAK in the control of VEGF-stimulated vascular permeability (Chen et al., 2012).

Here, we show that FAK directly phosphorylates VEC-Y658 and that intrinsic FAK activity controls VEC-Y658 phosphorylation downstream of VEGFR-2 and c-Src activation in vivo. Conditional FAK KD knockin within ECs prevents VEGF-enhanced tumor cell extravasation and spontaneous metastasis without effects on tumor growth. As FAK inhibition acts to maintain EC barrier function, these results support a distinct role for EC FAK activity in facilitating tumor spread.

Results

FAK is activated and promotes VEC-Y658 phosphorylation in tumor-associated ECs

Invasive ductal carcinoma is the most common form of breast cancer. Tumors can spread to lymph nodes and other parts of the body via intravasation into blood vessels. Staining of normal breast tissue with an antibody to a major FAK phosphorylation site (pY397 FAK) shows little reactivity in normal breast tissue, but strong staining of tumor and stromal blood vessels in invasive ductal carcinoma samples (Fig. 1 A). In an orthotopic, syngeneic BALB/c mouse breast carcinoma model (4T1-L), oral administration of a FAK-I (PND-1186) reduces primary tumor growth and spontaneous metastasis to the lung (Walsh et al., 2010). Analysis of 4T1-L tumor lysates shows inhibition of VEC-Y658 and FAK-Y397 phosphorylation upon FAK-I addition to mice as measured by phosphospecific antibodies to these sites (Fig. 1, B and C). As VEC-Y658 phosphorylation is implicated in the regulation of EC barrier function (Potter et al., 2005; Dejana et al., 2009), these data suggest a role for FAK in this control. Additionally, the adherens junction protein β-catenin is expressed in both ECs and tumor cells, and phosphorylation at β-catenin Y142 in 4T1-L tumors is reduced by FAK-I

administration (Fig. S1 A). β-Catenin Y142 is a direct substrate of FAK (Chen et al., 2012).

In an orthotopic, syngeneic mouse ovarian carcinoma model (ID8-IP), oral administration of another FAK-I (PF-271) reduced tumor growth and spontaneous metastasis (Ward et al., 2013). Primary ID8-IP ovarian tumors are characterized by bloody ascites, peritoneal spread, and distant site metastasis (Fig. S1 B) in a similar pattern observed in late-stage human ovarian cancer (Obermayr et al., 2013). VEC is expressed in ECs but not ID8 cells (Fig. S1 C). Analysis of ID8-IP tumor lysates shows inhibition of VEC-Y658 and FAK-Y397 phosphorylation upon FAK-I addition to mice (Fig. 1, D and E; and Fig. S1 D). β-Catenin Y142 phosphorylation, but not c-Src activation (as measured by a phosphospecific antibody to the activation loop site, pY416 c-Src), is also reduced by FAK-I treatment of ID8-IP tumors (Fig. S1 E). EC-specific VEC-Y658 phosphorylation in tumors was verified by staining ID8-IP tumor sections (Fig. 1 F). In control tumors, VEC pY658 staining colocalizes with the CD31 EC marker. FAK-I treatment results in loss of VEC pY658 but not CD31 staining. FAK pY397 staining colocalizes with CD31, FAK pY397 is also detected in other cells within ID8-IP tumors, and FAK-I treatment eliminates FAK pY397 but not CD31 staining. Together, these results show that oral administration of two different FAK-Is block FAK-Y397 and VEC-Y658 phosphorylation in ECs within breast and ovarian tumors.

Genetic FAK inhibition prevents VEGF-stimulated VEC-Y658 phosphorylation in vivo and in vitro

To assess the role of FAK in vivo and bypass the lethality of inactive FAK expression (Lim et al., 2010; Zhao et al., 2010), we previously created a conditional KD FAK knockin within adult mouse ECs (Fig. S2 A; Chen et al., 2012). FAK-KD mice exhibit no basal vasculature alterations but show reduced dermal vascular permeability in response to VEGF (Chen et al., 2012). To investigate the role of EC FAK signaling in vivo, VEGF-A or PBS were tail vein injected, and lysates of mouse lungs or hearts were analyzed within 2 min (Fig. 2 A and Fig. S2, B and C). In FAK–wild-type (WT) mice, VEGF increased VEGFR-2 activation and VEC-Y658, FAK-Y397, and c-Src–Y416 phosphorylation. In FAK-KD mice, VEGF increased VEGFR-2 and c-Src–Y416 phosphorylation but not VEC-Y658 or FAK-Y397 phosphorylation (Fig. 2 A). Similar signaling differences were observed after VEGF stimulation of FAK-WT and FAK-KD primary mouse heart and lung ECs (mHLECs; Fig. 2 B and Fig. S1 C). Correspondingly, FAK-I addition to HUVECs blocked VEGF-stimulated VEC-Y658 and FAK-Y397 phosphorylation without effects on VEGFR-2 or c-Src–Y416 phosphorylation (Fig. 2 C). In cell culture, VEGF-stimulated increases in VEC-Y658, β-catenin Y142, and FAK-Y397 phosphorylation were rapid with maximal levels observed within 5–10 min (Fig. S2 D). Maximal FAK-dependent VEC-Y658 phosphorylation occurred within 15–30 min after TNF-α stimulation of HUVECs (Fig. S2 E). Importantly, a linkage between VEGF, FAK activity, and VEC-Y658 phosphorylation was also observed by immunofluorescent staining of lung blood vessels. Colocalization
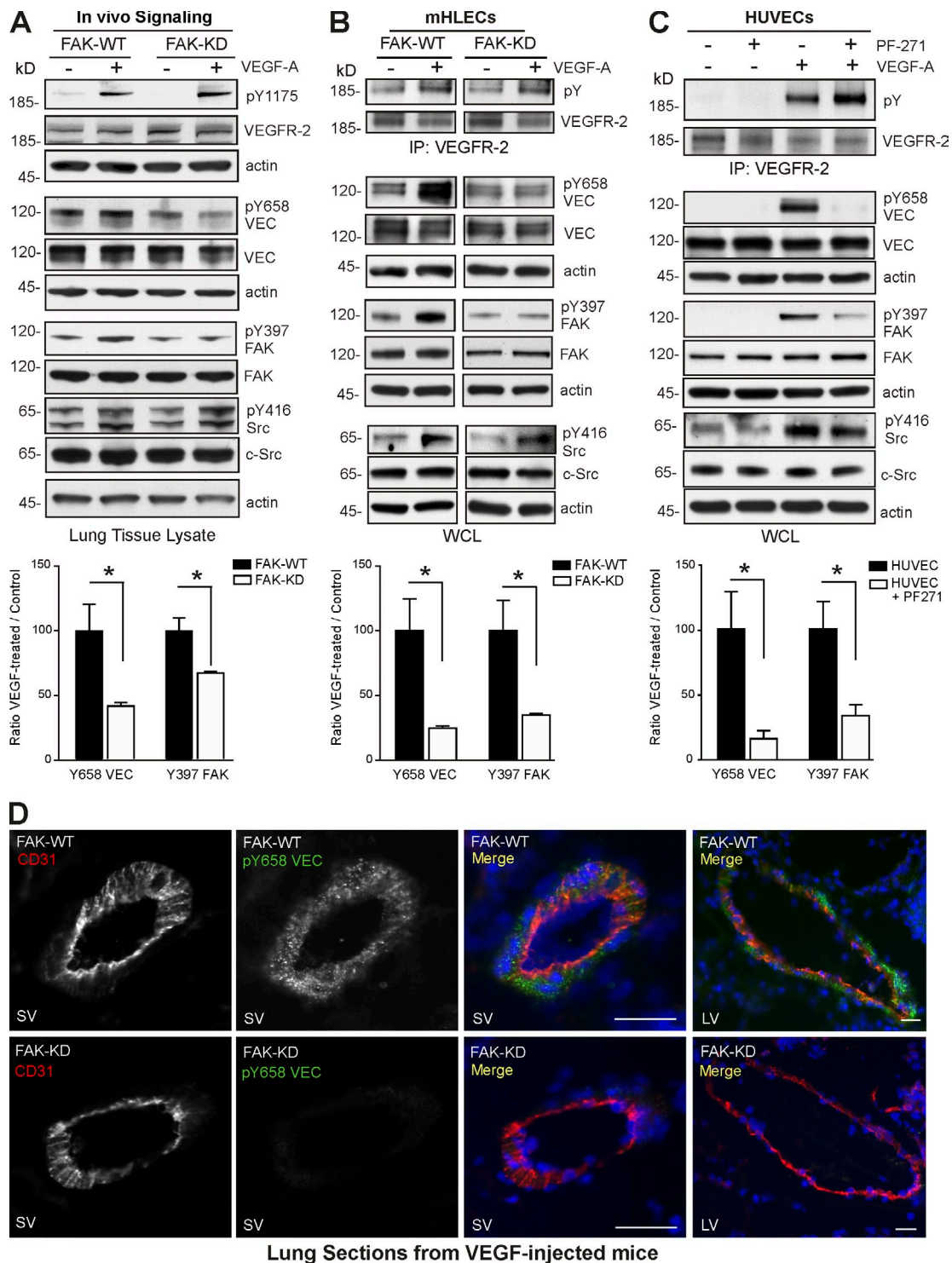
Figure 2. FAK-dependent VEGF-A stimulation of VEC-Y658 phosphorylation in lung tissue, primary mHLECs, and human ECs. (A, top) Lung lysates from FAK-WT or FAK-KD mice were analyzed 2 min after PBS or VEGF-A tail vein injections. Equal VEGFR-2 Y1175 phosphorylation occurs in FAK-WT and FAK-KD in response to VEGF. VEC pY658, FAK pY397, and c-Src pY416 were increased in VEGF-stimulated FAK-WT mice. Increased c-Src pY416, but not VEC pY658 or FAK pY397, were detected in VEGF-stimulated FAK-KD mice. Blots were reprobed for total VEGFR-2, VEC, FAK, and c-Src. Actin was used as a loading control. (bottom) Densitometry of VEC pY658 and FAK pY397 in lung lysates from FAK-WT or FAK-KD mice. Mean values are the ratio of pY658 VEC or pY397 FAK (normalized to total VEC or FAK) between VEGF-treated and control mice ± SEM from three independent experiments. Ratio of VEGF/control in FAK-WT mice was set to 100. (B) 50 ng/ml VEGF-A (10 min) equally activates VEGFR-2 but does not increase VEC pY658 in FAK-KD compared with FAK-WT mHLECs. Blotting and densitometry analyses were performed as described in A. (C) 1 µM PF-271 blocks 50 ng/ml VEGF-A–stimulated (10 min) VEC pY658 and FAK pY397 but not VEGFR-2 tyrosine phosphorylation or c-Src pY416 in HUVECs. Densitometry of VEC pY658 and FAK pY397 (normalized to total VEC or FAK) in VEGF/nontreated or VEGF/PF-271–treated HUVEC is obtained from three independent experiments. The ratio of VEGF/nontreated was set to 100. (A–C) Error bars are means ± SEM. *, P < 0.05. IP, immunoprecipitation; WCL, whole-cell lysate. (D) Lungs from VEGF-treated (2 min) FAK-WT or FAK-KD mice analyzed by combined staining for ECs (CD31) and VEC pY658. Merged images (DAPI nuclear stain, blue) show VEC pY658 costaining in association with ECs (yellow) in small vessels (SV) and large vessels (LV) in VEGF-treated FAK-WT but not FAK-KD mice. Bars, 30 µm.

of the CD31 EC marker and VEC pY658 staining was observed in lungs from FAK-WT, but not FAK-KD, mice tail vein injected with VEGF (Fig. 2 D). These results show that genetic or pharmacological FAK inhibition prevents VEC-Y658 phosphorylation downstream of VEGF-initiated VEGFR-2 or c-Src activation and that FAK activity may regulate VEC-Y658 phosphorylation in response to different stimuli.

FAK and c-Src activity coordinately regulate VEGF-stimulated FAK–c-Src translocation to adherens junctions

The importance of c-Src in mediating VEC tyrosine phosphorylation is supported by knockout and pharmacological inhibitor studies (Weis et al., 2004; Orsenigo et al., 2012). However, we find that FAK inhibition prevents VEC-Y658 phosphorylation without altering VEGF-stimulated c-Src activation (Fig. 2). To determine whether this effect is associated with modified c-Src intracellular localization, human pulmonary aortic ECs (HPAECs) were analyzed for activated c-Src (pY416 c-Src) and FAK distribution by immunofluorescent staining and confocal microscopy (Fig. 3). In starved (control) HPAECs, FAK exhibited a cytoplasmic and a punctate- or focal adhesion–associated staining pattern, whereas pY416 c-Src staining was generally low. Notably, VEGF addition (10 min) resulted in enhanced costaining of pY416 c-Src and FAK at cell–cell junctions in close proximity to VEC (Fig. 3, A–C). Addition of FAK (PF-271) or c-Src (Dasatinib) inhibitors to control HPAECs did not alter basal staining patterns. However, in the presence of VEGF, PF-271 prevented active pY416 c-Src accumulation with VEC at cell–cell junctions (Fig. 3, A and B) and promoted pY416 c-Src punctate staining that did not colocalize with FAK (Fig. 3 A). In the presence of Dasatinib + VEGF, FAK staining remained in a punctate–focal adhesion pattern and did not colocalize with VEC (Fig. 3, A and C). Thus, c-Src or FAK inhibitions mutually prevent VEGF-initiated adherens junction localization of active c-Src and FAK.

Immunoblotting showed that VEGF enhanced VEC pY658, FAK pY576/577 activation loop, FAK pY397, and c-Src pY416 activation loop site phosphorylation compared with starved cells (Fig. 3 D). Dasatinib lowered both basal and VEGF-stimulated VEC pY658, FAK pY576/577, and c-Src pY416 but not FAK pY397 phosphorylation (Fig. 3 D). This result is consistent with the need for c-Src activity in mediating full FAK activation in response to VEGF as measured by FAK pY576/577 phosphorylation. Similarly, Dasatinib prevents FAK colocalization with VEC in response to VEGF (Fig. 3 C). In addition, although FAK activity is not essential for VEGF-stimulated c-Src activation (Fig. 2), FAK-I prevents activated c-Src association with adherens junctions and VEC-Y658 phosphorylation. Together, these results support a linkage whereby FAK acts downstream of c-Src to coordinate VEGF-initiated redistribution of FAK–c-Src to adherens junctions leading to VEC pY658 phosphorylation.

Direct phosphorylation of VEC on pY658 by FAK

In vitro phosphorylation assays have demonstrated that c-Src can phosphorylate VEC at Y685 (Wallez et al., 2007), and indirect measures support the importance of c-Src in VEC-Y658

phosphorylation in vivo (Weis et al., 2004; Orsenigo et al., 2012). In vitro kinase assays using purified FAK, c-Src, and a GST fusion of the VEC cytoplasmic domain (amino acids 621–784) show that both FAK and c-Src phosphorylate GST-VEC at Y658 (Fig. 4 A). PF-271 addition inhibited FAK, but not c-Src, phosphorylation of GST-VEC at Y658, whereas PF-271 did not alter c-Src autophosphorylation at Y416 (Fig. 4 A). Mass spectrometry (MS) analyses revealed that FAK directly phosphorylated GST-VEC residues Y658, Y685, Y725, and Y757 in vitro (Fig. 4, B and C). These results show that VEC-Y658 is a direct substrate of FAK in vitro and that PF-271 does not directly prevent c-Src phosphorylation of VEC at Y658.

Tumor-associated VEGF-A triggers VEC-Y658 phosphorylation and transcellular migration dependent on EC FAK activity

Elevated VEGF-A expression occurs in breast (Arias-Pulido et al., 2012), ovarian (Masoumi Moghaddam et al., 2012), and melanoma (Palmer et al., 2011) tumors associated with advanced disease. To study the role of VEGF secreted by tumor cells on EC-associated signaling changes, murine VEGF-A secretion was quantified by ELISA (Fig. 5 A). Highly metastatic ovarian ID8-IP cells produce >40-fold elevated VEGF-A levels compared with parental ID8 cells. Stable overexpression of murine VEGF-A in ID8 cells (ID8-VEGF) was at an intermediate level (∼200 pg per million cells over 48 h) and equal to VEGF-A secretion from aggressive B16F10 melanoma cells (Fig. 5 A).

To evaluate the signaling effects of VEGF-expressing tumor cell adhesion to ECs, ID8 or ID8-VEGF cells were added to a monolayer of HUVECs in the presence or absence of PF-271 (Fig. 5 B). At 6 h, immunoblotting revealed increased VEGFR-2 activation and VEC-Y658 phosphorylation after ID8-VEGF addition compared with ID8 or no tumor cell addition to HUVECs. VEGFR-2, VEC, and CD31 are EC markers—not expressed in ID8 or ID8-VEGF cells (Fig. S1 C). FAK-Y397 (Fig. 5 B) and β-catenin Y142 (Fig. S3 A) phosphorylation were also enhanced upon ID8-VEGF compared with ID8 addition to HUVECs, and this was blocked by PF-271 addition. Notably, ID8 and ID8-VEGF addition elevated c-Src–Y416 phosphorylation, and this was not prevented by PF-271 (Fig. 5 B). Interestingly, total VEC levels in HUVECs were inversely proportional to VEC-Y658 phosphorylation (Fig. 5 B). PF-271 did not alter tumor cell adhesion to HUVECs (Fig. S3 B), but PF-271 prevented ID8-VEGF–triggered VEC-Y658 phosphorylation and maintained VEC expression levels independent of effects on VEGFR-2 activation (Fig. 5 B). These results show that interactions of VEGF-expressing tumor cells enhance VEC-Y658 phosphorylation within ECs in a FAK-dependent manner.

As VEC tyrosine phosphorylation is associated with enhanced internalization (Dejana et al., 2008), the role of FAK activity in the amount of antibody-bound VEC protected by acid wash conditions upon VEGF addition was determined (Fig. 5 C). VEGF addition triggered increased VEC uptake, and this was inhibited by PF-271. As point mutation of VEC-Y658 prevents internalization (Orsenigo et al., 2012), these results support the notion that FAK activity regulates VEC internalization in response to VEGF stimuli in part through the regulation of VEC-Y658 phosphorylation.
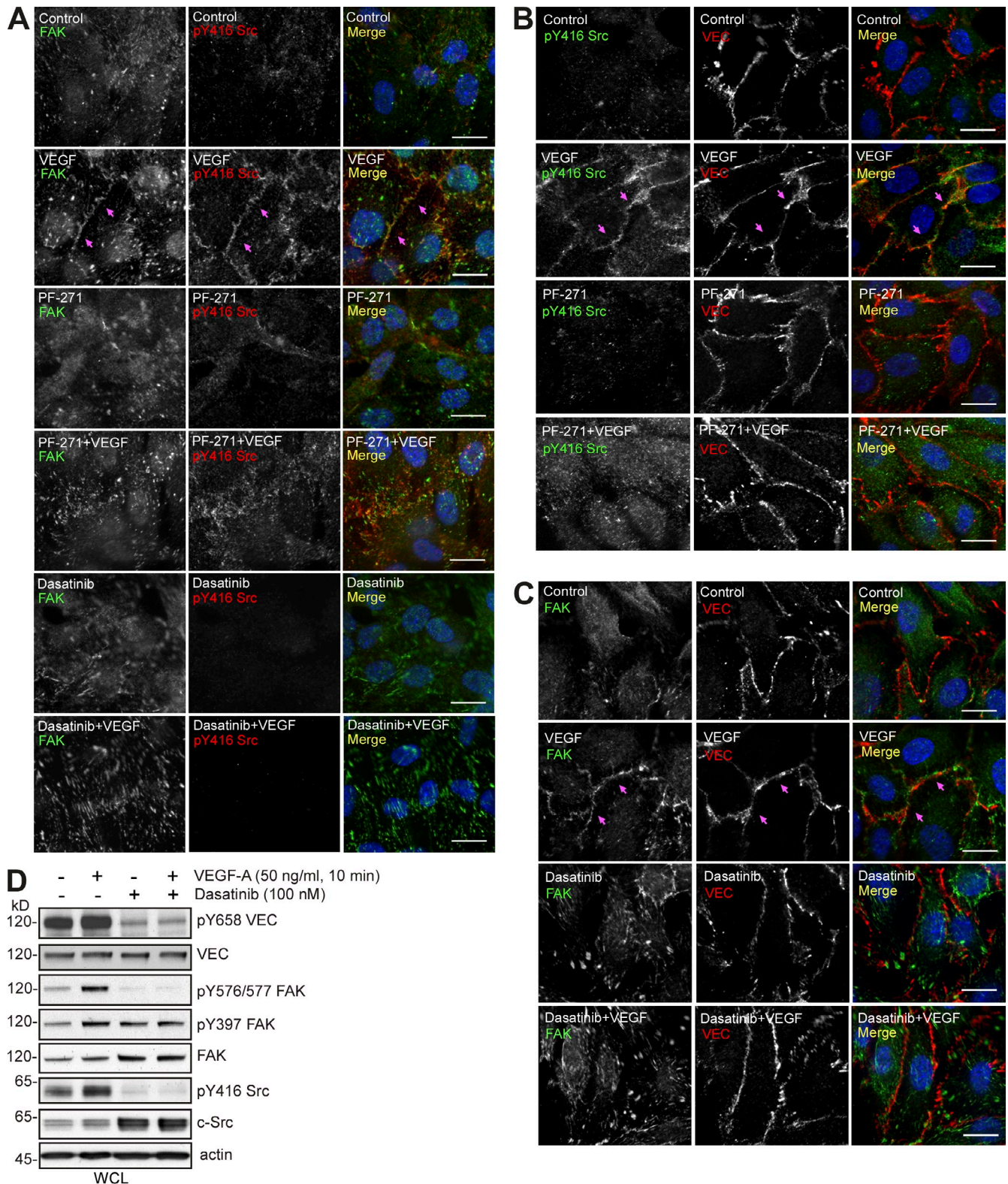
Figure 3. **Combined c-Src and FAK activity are required for VEGF-A–induced c-Src–FAK adherens junction localization.** (A–C) HPAEC immunofluorescent staining. Serum-starved cells were pretreated or not treated with 1 µM PF-271 or 100 nM Dasatinib for 1 h, fixed, or 50 ng/ml VEGF-A stimulated (10 min) and then fixed. (A) Combined staining for FAK and pY416 c-Src. (B) Combined staining for pY416 c-Src and VEC. (C) Combined staining for FAK and VEC. (A–C) Merged images (DAPI nuclear stain, blue) show staining colocalization (yellow). Arrows denote points of colocalization. Bars, 10 µm. (D) Dasatinib pretreatment inhibits VEGF-A–induced Y416 c-Src, FAK-Y576/577, and Y658 VEC phosphorylation but does not impact Y397 FAK phosphorylation as shown by immunoblotting whole-cell lysates (WCL). Blots were reprobed for total VEC, FAK, and c-Src. Actin is the loading control.
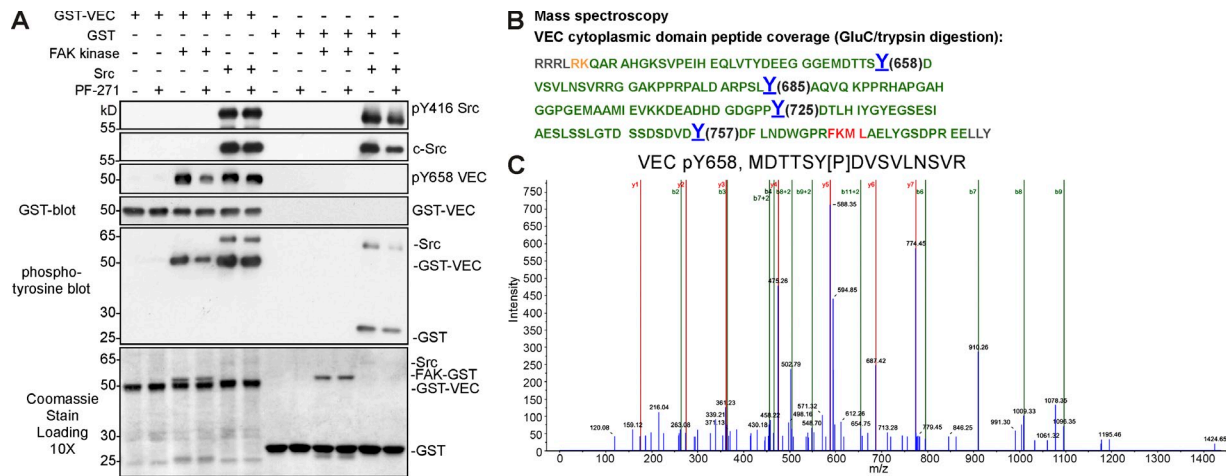
Figure 4. **FAK directly phosphorylates VEC-Y658.** (A) In vitro kinase assays with recombinant FAK kinase domain, full-length c-Src, and GST fusion protein of cytoplasmic VEC (GST-VEC 621–784) or GST alone. Assays were performed in the presence or absence of 0.5 µM PF-271. Immunoblotting was used to monitor c-Src pY416, total c-Src, VEC pY658, GST-VEC fusion, and phosphotyrosine incorporation. GST was not detectably phosphorylated by FAK, and Coomassie blue staining shows recombinant protein levels. (B) MS coverage of GST-VEC phosphorylation by FAK. Green, >95% confidence in the detected sequence; yellow, between 50 and 90% confidence; red, <50% confidence; gray, no detection. Blue, >99% paragon algorithm confidence score with a phosphorylated tyrosine present at the indicated position. (C) Analysis of the product scan for the ion 891.8829 (+2 charge state). The fragment ion masses correspond to fragmentation of peptide MDTTSY[P]DVSVLNSVR with a phosphorylated tyrosine at position Y658 (paragon algorithm confidence >99%). m/z, mass per charge.
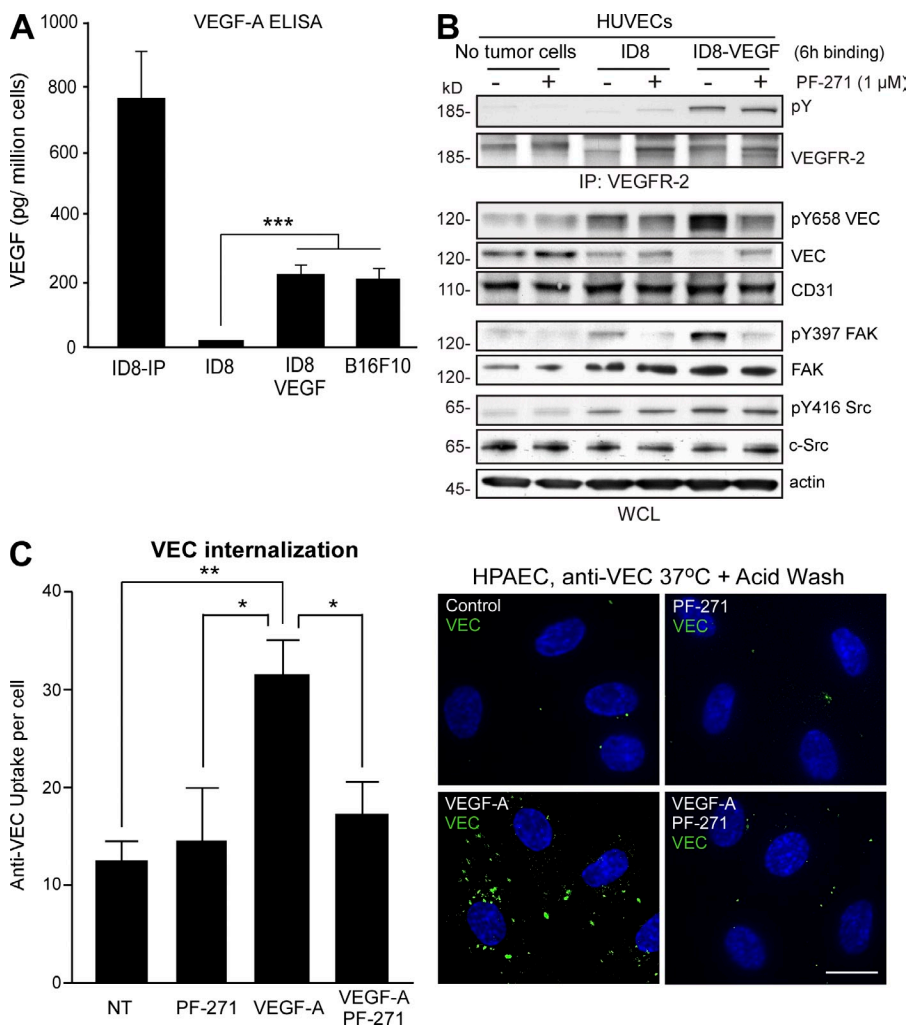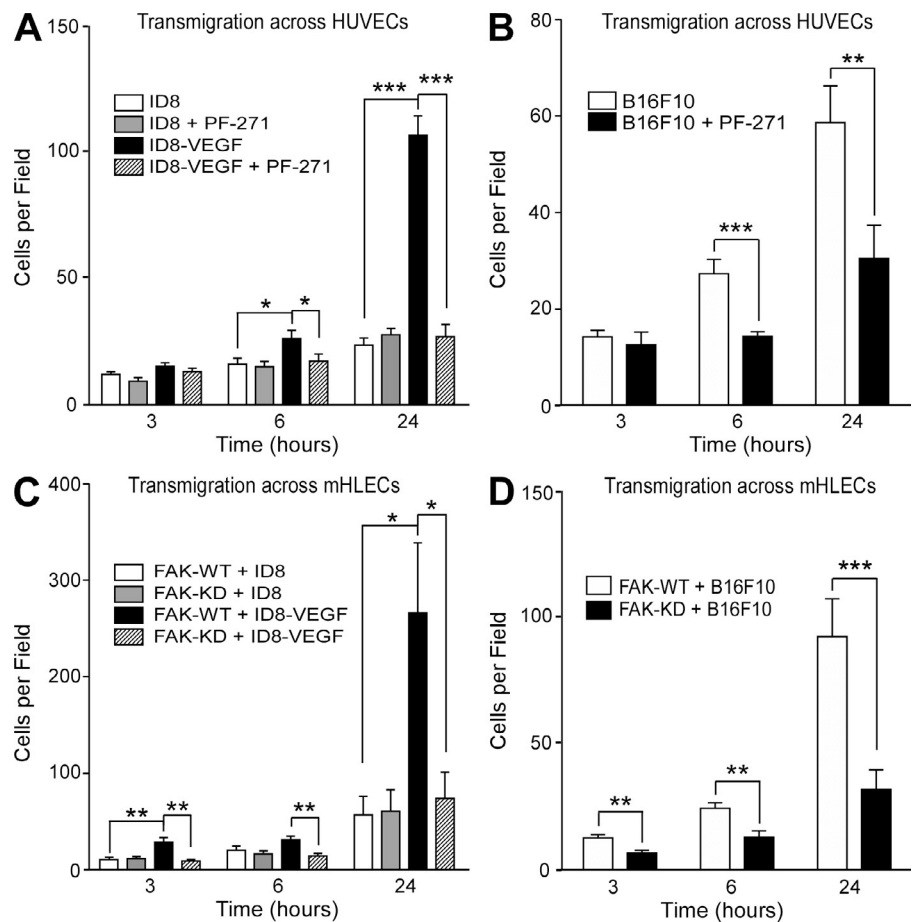

Figure 5. **Tumor-associated VEGF-A triggers VEC pY658 and VEC internalization dependent on EC FAK activity.** (A) VEGF-A ELISA from the indicated tumor cell conditioned media after 48 h. Values are means ± SEM from four independent experiments and normalized to tumor cell number (***, P < 0.001). (B) No cells (medium only is used as a control), ID8, or ID8-VEGF cells were added quiescently to a HUVEC monolayer (1:5 tumor cell to HUVEC ratio) for 6 h in the presence of 1 µM PF-271 or DMSO as indicated. Anti–VEGFR-2 immunoprecipitations (IP) were analyzed by phosphotyrosine (pY) immunoblotting and reprobed for total VEGFR-2. Whole-cell lysates (WCL) were analyzed by pY658 VEC, pY397 FAK, and pY416 c-Src and total VEC, FAK, and c-Src. CD31 is EC specific, and actin is the total loading control. (C) FAK activity regulates VEC internalization in response to VEGF. Starved HPAECs were incubated with an antibody to the VEC extracellular domain, treated with 1 µM PF-271, and/or stimulated with VEGF-A (30 min). Acid wash–resistant anti-VEC antibody internalization was visualized by fluorescence microscopy, quantified using ImageJ, and expressed as points of anti-VEC uptake per cell (n ≥ 400 cells, three independent experiments; means ± SEM; *, P < 0.05; **, P < 0.01 by analysis of variance). NT, not treated. (right) Representative images with anti-VEC and nuclei stained with DAPI (blue). Bar, 10 µm.

Figure 6. **Tumor-associated VEGF-A triggers transcellular migration dependent on EC FAK activity.** (A and B) Transmigration of fluorescently labeled ID8 and ID8-VEGF ovarian (A) or B16F10 melanoma (B) tumor cells across the HUVEC monolayer in the presence of 1 µM PF-271 as indicated and analyzed at 3, 6, and 24 h. (C and D) Transmigration of fluorescently labeled ID8 and ID8-VEGF ovarian (C) or B16F10 melanoma (D) tumor cells across FAK-WT or FAK-KD mHLECs as indicated and analyzed at 3, 6, and 24 h. (A–D) Values are means ± SEM from three independent experiments of triplicates (*, P < 0.05; **, P < 0.01; ***, P < 0.001).

A previous study showed that FAK activity was essential for VEGF-stimulated vascular permeability (Chen et al., 2012). As VEC supports EC contact integrity and barrier formation, tumor cell transmigration analyses across a HUVEC monolayer were performed with ID8, ID8-VEGF, or B16F10 cells in the presence or absence of PF-271 (Fig. 6, A and B). Increased ID8-VEGF transcellular migration occurred at 6 and 24 h compared with ID8 cells (Fig. 6 A). PF-271 prevented ID8-VEGF and B16F10 melanoma transmigration across HUVECs at 6 and 24 h (Fig. 6, A and B) without affecting adhesion (Fig. S3 B). Because PF-271 may inhibit tumor cell motility (Roberts et al., 2008), transmigration assays were performed using FAK-WT and FAK-KD mHLECs as a barrier (Fig. 6, C and D). Increased ID8-VEGF and B16F10 transcellular migration occurred across FAK-WT compared with FAK-KD mHLECs at 3, 6, and 24 h. As no differences were observed for ID8-VEGF or B16F10 adhesion to FAK-WT or FAK-KD mHLECs (Fig. S3 C), these results indicate that VEGF-stimulated tumor cell transmigration is dependent on EC FAK activity.

Selective importance of VEC-Y658 phosphorylation in VEGF-initiated paracellular permeability and tumor cell transmigration

VEC is phosphorylated at several tyrosine sites within the cytoplasmic domain. VEC tyrosine to phenylalanine (Y to F) mutations at positions 645, 731, or 733 inhibit lymphocyte transmigration across reconstituted VEC-null mouse endothelioma cells (Turowski et al., 2008). Whereas VEC-Y658F or Y685F mutations did not prevent lymphocyte transmigration, these mutations inhibited bradykinin-triggered paracellular permeability (Orsenigo et al., 2012).

To evaluate the role of VEC tyrosine phosphorylation in VEGF-induced tumor cell transmigration, VEC-null ECs (Carmeliet et al., 1999) were stably reconstituted with VEC-WT, VEC-Y658F, VEC-Y685F, or VEC-Y733F as GFP fusion proteins (Fig. 7 A). WT and Y to F point mutant VEC proteins localized to cell–cell junctions (Fig. 7 B), whereas GFP alone was cytoplasmic (Fig. S4 A). VEC-WT and Y to F point mutations were stably and equivalently expressed (Fig. 7 C). VEGFR-2 was equally activated by VEGF-A in VEC-WT–, -Y658F–, -Y685F–, and -Y733F–expressing ECs (Fig. S4 B), and VEGF-A–initiated paracellular permeability at 15 min was increased to the same extent in VEC-WT–, -Y685F–, and -Y733F–expressing ECs (Fig. 7 D). However, VEC-Y658F ECs exhibited significantly reduced VEGF-A paracellular permeability (Fig. 7 D). Notably, Y658F VEC mutation prevented ID8-VEGF and B16F10 transmigration at 6 and 24 h compared with VEC-WT ECs (Fig. 7, E and F). Expression of VEC-Y685F and VEC-Y733F mutations did not alter ID8-VEGF or B16F10 transmigration compared with VEC-WT–reconstituted ECs. As ID8-VEGF and B16F10 (Fig. S4, C and D) adhesion was equivalent between VEC-WT– and point mutation–reconstituted ECs, these results support the
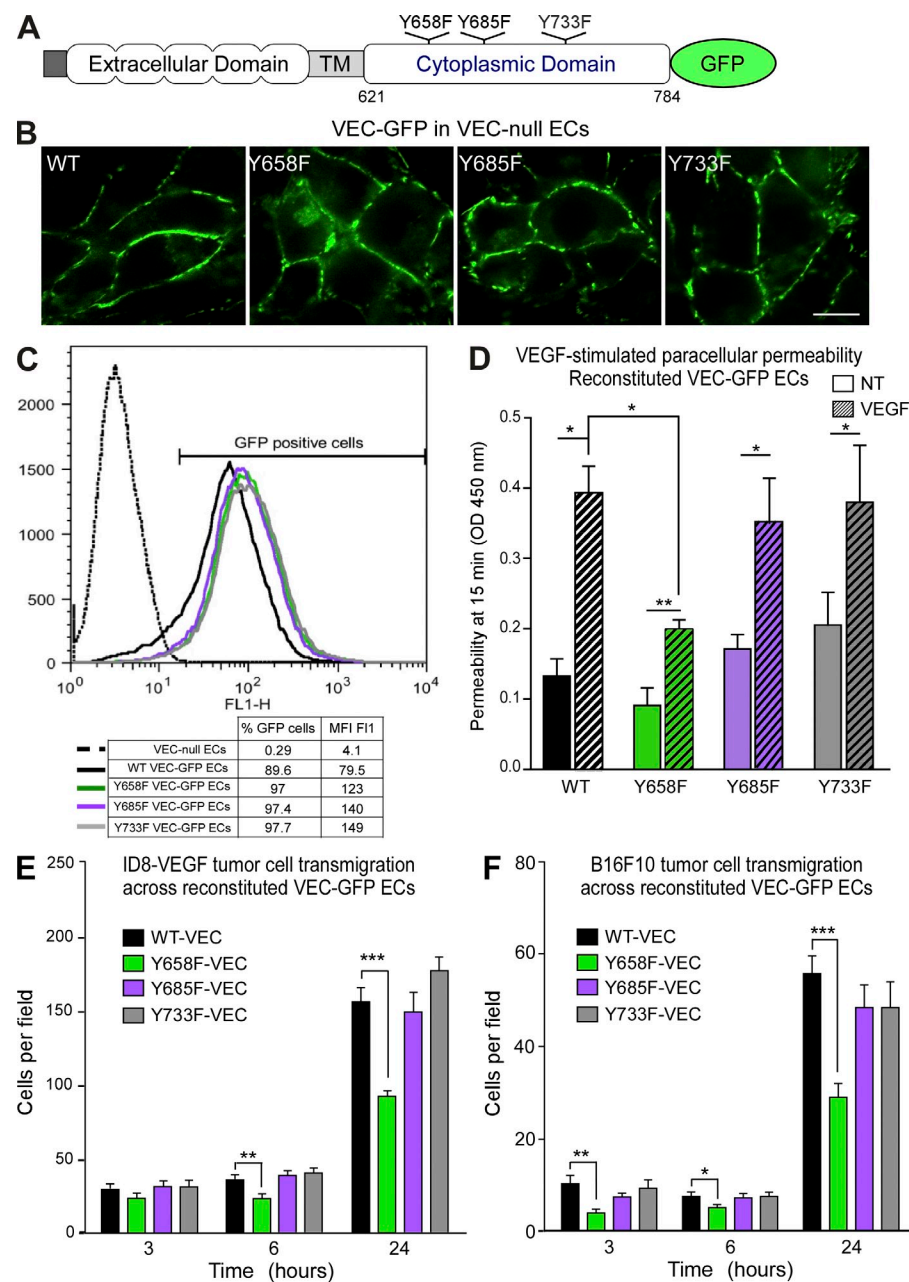
Figure 7. **Selective importance of VEC-Y658 phosphorylation in VEGF-stimulated paracellular permeability and tumor cell transmigration.** (A) VEC schematic showing extracellular, transmembrane (TM), and cytoplasmic domain with location of Y658F, Y685F, and Y733F point mutations fused to GFP. (B) Localization of the indicated VEC-GFP constructs to cell–cell junctions in VEC-null ECs. Bar, 10 µm. (C) Flow cytometry shows equivalent VEC-GFP WT, Y658F, Y685F, and Y733F expression in ~90% of VEC-null ECs. 10,000 cells were analyzed for each condition. Data shown are from a single representative experiment out of three repeats. (bottom) Table showing enumeration of GFP-positive (expressed as percentages) cells and mean fluorescence intensity (MFI). (D) Basal (NT, no treatment) and 100 ng/ml VEGF-A (15 min)–stimulated paracellular permeability measured in confluent cultures of VEC-null ECs reexpressing VEC-WT, VEC-Y658F, VEC-Y685F, or VEC-Y733F. Values are means ± SEM from four independent experiments of triplicates (*, P < 0.05; **, P < 0.01). (E and F) Transmigration of fluorescently labeled ID8-VEGF ovarian (E) or B16F10 melanoma (F) tumor cells across confluent cultures of VEC-null ECs reexpressing VEC-WT, VEC-Y658F, VEC-Y685F, and VEC-Y733F and analyzed at 3, 6, and 24 h. Values are means ± SEM from three independent experiments of triplicates (*, P < 0.05; **, P < 0.01; ***, P < 0.001).

selective importance of VEC-Y658 phosphorylation in promoting VEGF-enhanced paracellular permeability and tumor cell transmigration.

Genetic FAK inhibition in ECs prevents VEGF-associated tumor cell extravasation and VEC-Y658 phosphorylation in vivo

FAK inhibition prevents melanoma (Li et al., 2007), breast (Walsh et al., 2010), and ovarian (Ward et al., 2013) tumor metastasis. Although proposed as a tumor cell–associated response (Mitra et al., 2006; Pylayeva et al., 2009), FAK signaling within ECs may also contribute to tumor cell escape from blood circulation. Initial tumor cell adhesion in the pulmonary microcirculation occurs rapidly. Clearance occurs between 6 and 16 h, and cells remaining after 16 h are either tightly adhered to the endothelium or have undergone extravasation (Labelle and

Hynes, 2012). After tail vein injection, equal numbers of ID8 or ID8-VEGF cells were present in the lungs after 6 h (Fig. 8 A). However, 16 h after injection, significantly increased ID8-VEGF cells were present in the lungs compared with ID8 (Fig. 8 B). This is consistent with VEGF-A in promoting ID8 tumor cell extravasation.

To test the role of EC FAK activity in the processes of cell adhesion and extravasation within lung vessels, ID8-VEGF tumor cells were tail vein injected into FAK-WT or FAK-KD mice, and at 6 h, equal numbers of tumor cells were present in the lungs (Fig. 8 C). Thus, initial tumor cell homing and adhesion were not affected by EC-specific FAK inhibition. However, by 16 h, significantly fewer tumor cells remained in the lungs of FAK-KD compared with FAK-WT mice (Fig. 8, D and E). Similar results were obtained after injecting B16F10 melanoma cells into FAK-WT and FAK-KD mice (Fig. 8, F and G). These
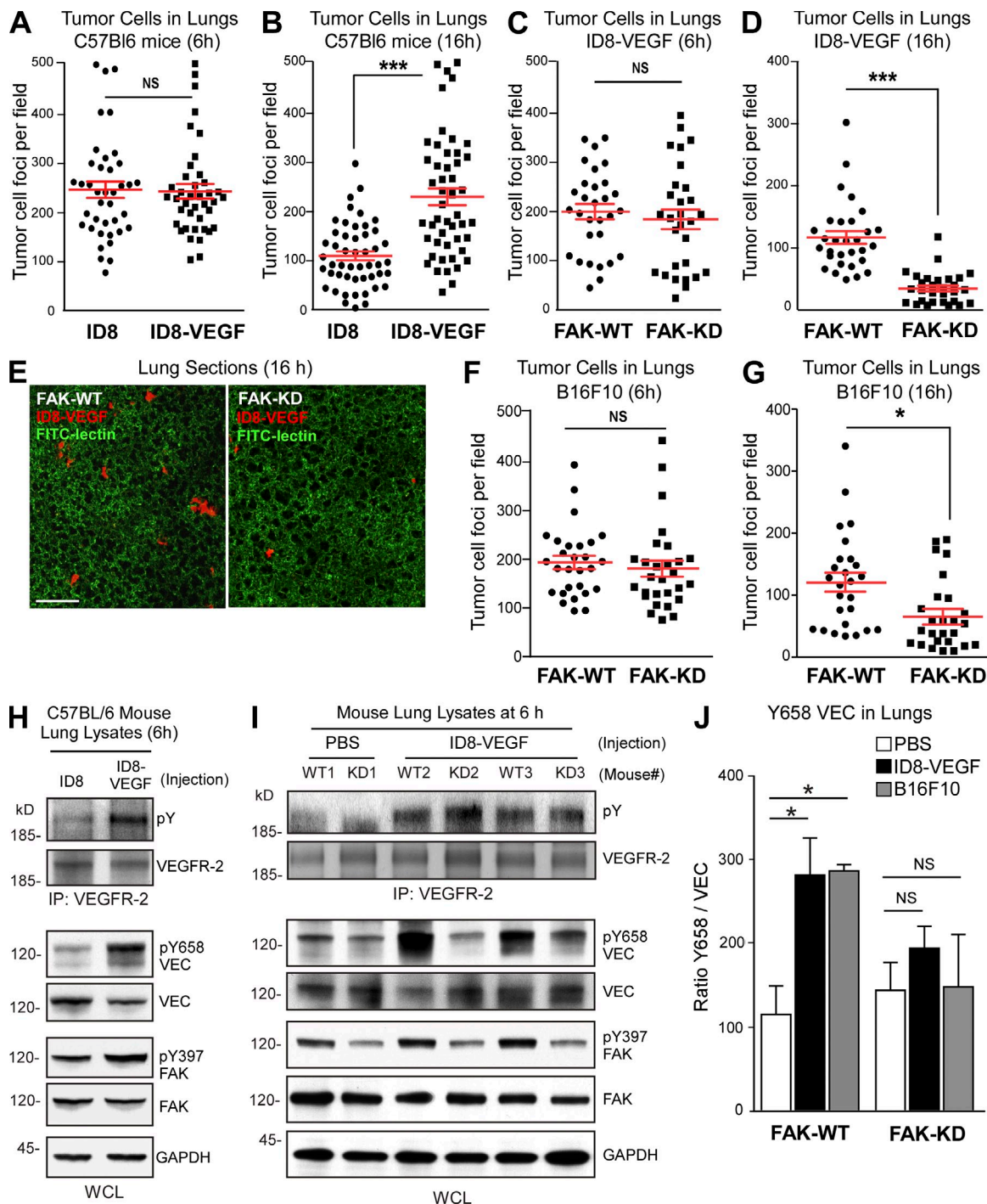
Figure 8.   **Genetic FAK inhibition in ECs prevents VEGF-enhanced tumor cell extravasation and VEC-Y658 phosphorylation in vivo.** (A and B) VEGF-A enhances ID8 tumor cell extravasation. Fluorescently labeled ID8 or ID8-VEGF cells were tail vein injected into C57BL/6 mice, and after 6 h (A) or 16 h (B), tumor cell foci were enumerated in the lung tissue. Values (red bars) are means ± SEM (***, P < 0.001). (C and D) Inhibition of ovarian tumor cell extravasation in FAK-KD mice. Fluorescently labeled ID8-VEGF cells were tail vein injected into FAK-WT or FAK-KD mice, and after 6 h (C) or 16 h (D), tumor cell foci were enumerated in lung tissue. Values (red bars) are means ± SEM (***, P < 0.001). (E) Representative lung section images from FAK-WT and FAK-KD mice from analyses in D. ID8-VEGF ovarian carcinoma cells were prelabeled with DilC12(3), and blood vessels were in situ labeled by FITC-lectin. Bar, 100 µm. (F and G) Inhibition of melanoma cell extravasation in FAK-KD mice. Fluorescently labeled B16F10 cells were tail vein injected into FAK-WT or FAK-KD mice, and after 6 h (F) or 16 h (G), tumor cell foci were enumerated in lung tissue. Values (red bars) are means ± SEM (*, P < 0.05). (H) In vivo signaling. C57BL/6 mice were tail vein injected with ID8 or ID8-VEGF tumor cells, and after 6 h, lung lysates were evaluated by VEGFR-2 immunoprecipitations (IP), phosphotyrosine (pY), and VEGFR-2 blotting. VEC pY658 and FAK pY397 immunoblotting were performed on lung lysates, and blots were sequentially reprobed for total VEC and FAK. GAPDH is the loading control. WCL, whole-cell lysate. (I) Inhibition of VEC pY658 in vivo. FAK-WT or FAK-KD mice were tail vein injected with ID8-VEGF cells or PBS (control), and lung protein lysates were made after 6 h. Independent samples (WT1–3) and (KD1–3) from different mice were evaluated by VEGFR-2 immunoprecipitations, pY, and VEGFR-2 blotting. VEC pY658 and FAK pY397 immunoblottings were performed on lung lysates, and blots were sequentially reprobed for total VEC and FAK. GAPDH is the loading control. (J) Densitometry of VEC pY658 lung lysate immunoblots from FAK-WT and FAK-KD injected with PBS, ID8-VEGF, or B16F10 tumor cells. Values are a mean ratio (pY658/total VEC) ± SEM from four independent lungs per experimental point. FAK-WT1–PBS was set to 100. (*, P < 0.05).

results support the notion that tumor cell–initiated signaling differences may exist within the vessels of FAK-KD mice.

To determine whether VEGF expression from ID8 cells was sufficient to initiate a signaling response in vivo, ID8 and ID8-VEGF cells were tail vein injected, and lung lysates were evaluated by immunoblotting after 6 h, a time of equal cell adherence within the lung microvasculature. Importantly, neither ID8 nor ID8-VEGF expresses VEGFR-2 or VEC (Fig. S1 C), so these proteins are from lung tissue. ID8-VEGF cells triggered increased VEGFR-2 activation, VEC-Y658, and FAK-Y397 phosphorylation at 6 h compared with ID8 injection in C57BL/6 mice (Fig. 8 H). To evaluate whether this signaling response was dependent on FAK activity, ID8-VEGF cells were injected into FAK-WT and FAK-KD mice. Compared with PBS injection controls, equally increased VEGFR-2 tyrosine phosphorylation was detected by ID8-VEGF injection at 6 h in both FAK-WT and FAK-KD mice (Fig. 8 I). However, VEC-Y658 phosphorylation was significantly reduced in FAK-KD compared with FAK-WT mice after ID8-VEGF or B16F10 injection after 6 h (Fig. 8, I and J). These results show that although equivalent VEGFR-2 activation occurs upon tumor cell adhesion within lung microvessels, genetic inactivation of FAK activity within ECs prevents VEC-Y658 phosphorylation and VEGF-induced tumor cell extravasation.

EC FAK inhibition prevents tumor metastasis without impacting tumor growth

As B16F10 melanoma-induced in vivo VEC-Y658 phosphorylation and lung vessel extravasation after 16 h were reduced in FAK-KD compared with FAK-WT mice (Fig. 8), experimental metastasis analyses were extended to 14 d (Fig. 9). B16F10 cells injected into FAK-KD mice exhibited fewer pulmonary macrometastases (Fig. 9, A and B), and tumor-associated FAK-KD mice had a lower total lung mass (Fig. 9 C) compared with B16F10-injected FAK-WT mice. Interestingly, when measuring total B16F10 metastatic lung nodule size, there was no difference between FAK-KD and FAK-WT mice (Fig. 9 D). One potential explanation for this result is that once B16F10 tumor cells had established colonies within lungs of FAK-WT and FAK-KD mice, tumor growth proceeded at an equivalent rate. To this end, when directly implanted subcutaneously in flanks of FAK-WT and FAK-KD mice, B16F10 cells grew equivalently as tumors over 20 d (Fig. 9 E). However, B16F10 cells do not readily metastasize as flank tumors; in contrast, spontaneous B16F10 dermal to lung metastasis occurs when injected orthotopically between the skin and cartilage of the ear (Bobek et al., 2010). In FAK-WT and FAK-KD mice, fluorescently labeled orthotopic B16F10 tumors were localized near the injection site (Fig. 9 F) and did not exhibit differences in tumor size after 21 d (Fig. 9 G). Importantly, a greater number of fluorescently labeled B16F10 tumor cells were visualized in the lungs of FAK-WT compared with FAK-KD mice after 21 d (Fig. 9, H and I). Together, these results show that EC FAK activity can impact the processes of spontaneous B16F10 tumor metastasis independent of alterations in primary tumor growth.

Discussion

FAK is a cytoplasmic tyrosine kinase that integrates cell survival and motility signals from growth factor and integrin cell surface receptors. As FAK-Is are being tested in clinical trials (Infante et al., 2012), it is important to understand that FAK signaling likely plays distinct roles in tumor versus stromal cell biology. Herein, we elucidate a new mechanism for EC FAK activity in the regulation of blood vessel barrier integrity and the passage of tumor cells through an EC barrier. Our studies were primarily focused on ovarian and melanoma tumor cell models that alter the tumor microenvironment in part by secreting VEGF-A. Using a tamoxifen-inducible mouse model with selective KD expression in ECs, we provide genetic and complementary pharmacological FAK-I results showing that FAK activity controls VEGF-stimulated VEC-Y658 phosphorylation in vitro and in vivo. Moreover, our experiments identify EC FAK as a key intermediate between VEGFR-2, c-Src, and the regulation of EC barrier function controlling tumor metastasis.

Interestingly, although EC FAK inhibition decreased experimental and spontaneous metastasis, this did not alter syngeneic B16F10 melanoma tumor growth in either flank or ear orthotopic models. This lack of a connection between EC FAK activity and tumor growth is unexpected, as conditional FAK deletion within ECs prevents glioma and B16F10 tumor growth associated with decreased angiogenesis and increased EC apoptosis (Lee et al., 2010; Tavora et al., 2010). One explanation is that there are fundamental differences between loss of FAK and kinase-inactive FAK (FAK-KD) expression that retains cytoplasmic and nuclear scaffolding functions (Lim, 2013). To this end, FAK knockout triggers increased EC apoptosis (Shen et al., 2005), whereas FAK-KD does not (Lim et al., 2010; Chen et al., 2012). Herein, we show that FAK-KD prevents tumor cell–stimulated VEC-Y658 phosphorylation in vivo and in vitro. This FAK-dependent connection to VEC-Y658 phosphorylation was recapitulated by analyses of recombinant VEGF-A–stimulated signaling within lung and heart tissue and primary mHLECs. As FAK controls β-catenin Y142 phosphorylation in response to VEGF and VEC-Y658 phosphorylation in response to VEGF and TNF, our results support the importance of FAK activity in the regulation of cell–cell adherens junctions in addition to the canonical role for FAK in controlling cell–matrix focal adhesion dynamics.

Posttranslational VEC modifications trigger junctional changes and VEC internalization (Dejana et al., 2008; Le Guelte et al., 2011). VEC-Y658 is located within the p120-catenin binding region, and mutagenesis results support a model whereby Y658 phosphorylation promotes VEC–p120-catenin dissociation and adherens junction breakdown (Potter et al., 2005). Stabilizing the VEC–catenin linkage lessens leukocyte extravasation and vascular permeability (Schulte et al., 2011). Although VEC-Y658F prevented neutrophil transendothelial migration (Allingham et al., 2007) and bradykinin-induced permeability (Orsenigo et al., 2012), VEC-Y658F did not alter ICAM-1–induced lymphocyte transmigration (Turowski et al., 2008). These studies support a model whereby cell-, receptor-,
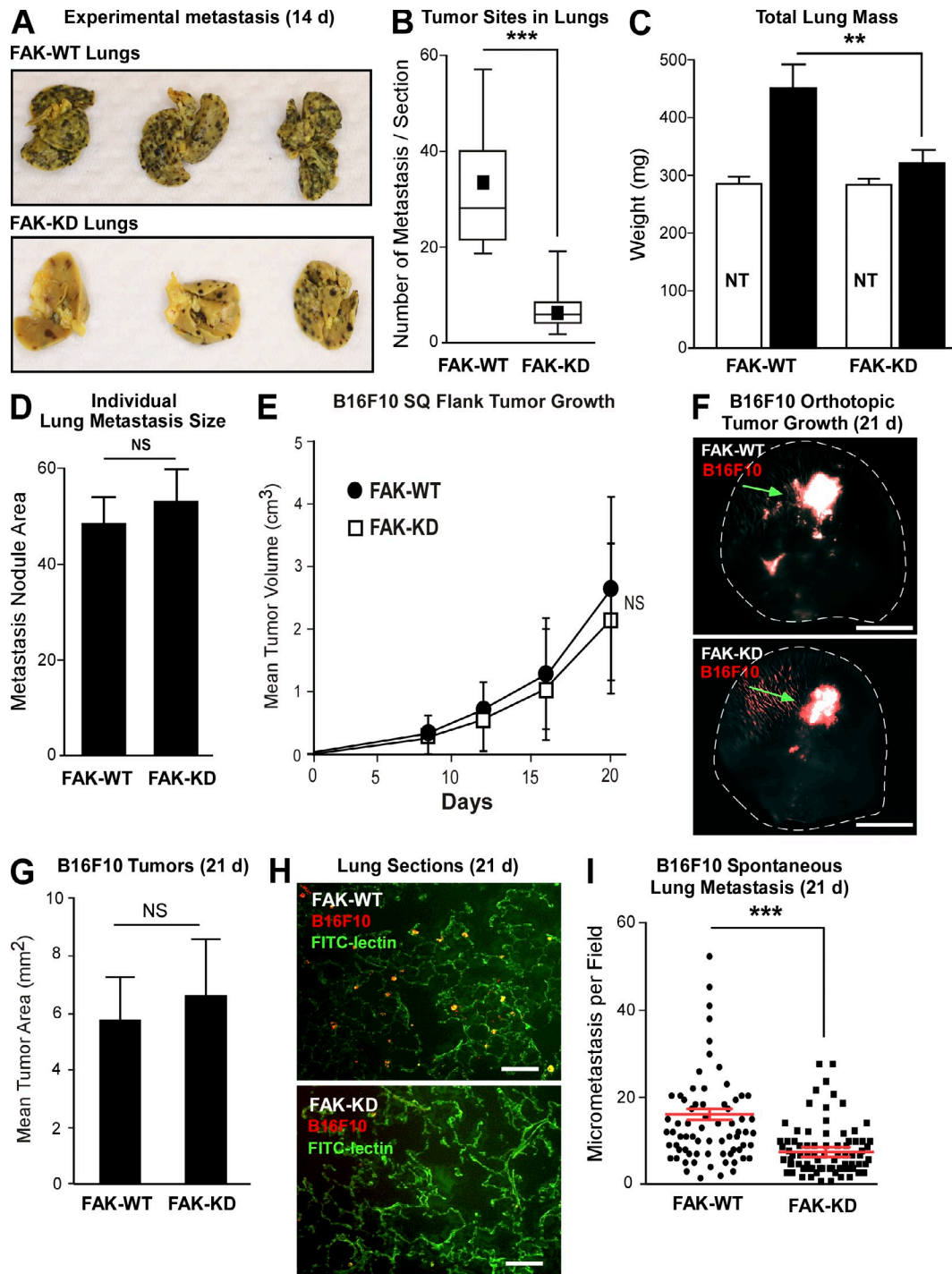
Figure 9. **Inhibition of B16F10 spontaneous tumor metastasis but not primary tumor growth in FAK-KD mice.** (A–D) B16F10 cells were tail vein injected into FAK-WT or FAK-KD mice, and lungs were evaluated after 14 d. (A) Representative Bouin's-stained lung images. B16F10 cells are dark from melanin production. (B) Metastatic B16F10 tumor sites were enumerated in H&E-stained lung sections from FAK-WT and FAK-KD mice. Box–whisker plots show the distribution of the data: black square, mean; bottom line, 25th percentile; middle line, median; top line, 75th percentile; and whiskers, fifth and 95th percentiles (***, $P < 0.001$). (C) Mean total lung mass ± SD from FAK-WT ($n = 11$) and FAK-KD ($n = 10$) mice injected with B16F10 cells (**, $P < 0.01$; black bars) and lung mass from nontumor (NT)-bearing mice. (D) Mean area of individual B16F10 lung metastases from FAK-WT and FAK-KD mice were measured using ImageJ from H&E-stained lung sections. Means ± SEM. (E) B16F10 subcutaneous tumor growth over 20 d in FAK-WT ($n = 11$) and FAK-KD ($n = 16$ mice). Values are means ± SD. (F–I) DsRed-labeled B16F10 melanoma cells were injected between the skin and the cartilage on the dorsal side of FAK-WT and FAK-KD mouse ears. Primary tumor growth and lung metastasis were evaluated after 21 d. (F) Representative fluorescent images of tumors on the ears of FAK-WT and FAK-KD mice. Arrows indicate the approximate B16F10 injection sites, and ears are encircled (dotted lines). Bars, 3 mm. (G) B16F10 primary tumor size in FAK-WT ($n = 10$) and FAK-KD ($n = 9$) mice. Values are means ± SEM. (H) Representative lung section images from FAK-WT and FAK-KD mice. Blood vessels were in situ labeled by FITC-lectin, and B16F10 melanoma cells were visualized by intrinsic fluorescence (DsRed). Bars, 100 µm. (I) Spontaneous B16F10 lung micrometastasis in FAK-WT and FAK-KD mice. 10 lung sections per mouse were enumerated, and values (red bars) are means ± SEM (***, $P < 0.001$).

or ligand-specific signaling may induce site-selective modulation of VEC affecting adherens junction stability.

We found that pharmacological FAK inhibition prevented VEGF-stimulated VEC internalization. Stable reexpression of VEC-Y658F in VEC-null ECs (but not Y685F or Y733F VEC mutations) reduced VEGF-induced permeability under conditions of equal VEGFR-2 activation. Moreover, VEC-Y658F mutation inhibited ID8-VEGF and B16F10 transmigration across VEC-reconstituted ECs. As genetic inactivation of FAK activity limits VEGF-induced VEC-Y658 phosphorylation and tumor cell transmigration, our results define FAK as an important intermediate between VEGFR-2 and the regulation of EC barrier function.

Similarly, knockout and pharmacological inhibitor studies have identified the c-Src tyrosine kinase as a key intermediate enhancing EC permeability via increased VEC and β-catenin phosphorylation (Weis et al., 2004; Orsenigo et al., 2012). VEGFR-2 activates c-Src in part through a complex with the T cell–specific adaptor protein (Sun et al., 2012), and we find that c-Src activation is not affected by either genetic or pharmacological FAK inactivation. This places FAK downstream of c-Src, but the mechanisms controlling VEGF-stimulated FAK activation remain unresolved. A previous study has shown that VEGF-stimulated FAK-Y397 phosphorylation may occur independently of VEGF-initiated and c-Src–mediated phosphorylation of FAK on other sites (Abu-Ghazaleh et al., 2001). Notably, we find that pharmacological c-Src inhibition by Dasatinib treatment prevents VEGF-stimulated FAK translocation to adherens junctions, FAK activation loop phosphorylation at Y576/Y577, and VEC-Y658 phosphorylation.

This result is consistent with the need for c-Src activity in mediating full FAK activation in response to VEGF as measured by FAK pY576/577 phosphorylation. Moreover, Dasatinib did not block VEGF-enhanced FAK phosphorylation at Y397 as did genetic or pharmacological FAK inhibition. Another study has also reported that FAK-Y397 phosphorylation is insensitive to Dasatinib treatment in HUVECs (Liang et al., 2010). These results underscore the complexity of the FAK activation process that is highly dependent on conformational changes occurring within the FAK N-terminal FERM (4.1 protein, ezrin, radixin, and moesin) domain (Lietha et al., 2007; Chen et al., 2012; Choi et al., 2013).

Finally, we found that pharmacological FAK inhibition also prevented the translocation of active c-Src to adherens junctions in response to VEGF. Thus, c-Src or FAK inhibition prevents VEGF-initiated adherens junction localization of active c-Src and FAK. Our results support a model whereby FAK acts downstream of c-Src to coordinate VEGF-initiated redistribution of FAK–c-Src to adherens junctions, leading to VEC pY658 phosphorylation. This view is consistent with the existing literature on the importance of c-Src activity in adherens junction regulation. However, further studies are needed to elucidate whether c-Src and FAK act sequentially, in parallel, or as a signaling complex for the modulation of adherens junction tyrosine phosphorylation in response to VEGF.

Overall, our results support a key role for FAK in the regulation of barrier function through site-specific tyrosine phosphorylation of adherens junction proteins in response to VEGF affecting tumor cell transmigration across the endothelium. In general, our observations support therapeutic approaches targeting FAK activity to prevent metastatic tumor spread by modifying EC signals regulating barrier function.

Materials and methods

Mice
Mice with loxP sites flanking FAK exon 3 (FAK$^{fl/fl}$) and a tamoxifen-inducible Cre–estrogen receptor tamoxifen (ER(T)) fusion protein (Cre-ER(T)) transgene downstream of the 5′ endothelial enhancer of the stem cell leukemia locus (Weis et al., 2008) were crossed with heterozygous mice containing a KD (FAK-KD/WT) knockin mutation within FAK exon 15 (available from the NCBI Nucleotide database under accession no. NC_000081; Lim et al., 2010). At 6 wk of age, FAK$^{fl/KD}$ Cre-ER(T) (designated FAK-KD) and FAK$^{fl/WT}$ Cre-ER(T) (designated FAK-WT) mice were treated with 2 mg tamoxifen (Sigma-Aldrich) every 2 d (i.p. injection in corn oil) for 2 wk (Chen et al., 2012). Experiments used littermates at 10 wk. The University of California, San Diego Institutional Animal Care and Use Committee approved all animal procedures.

Cells
Murine B16F10 melanoma (CRL-6475) and 4T1 breast carcinoma were obtained from ATCC. 4T1-L cells were derived from 4T1 lung metastatic cells selected by growth in 6-thioguanine (Sigma-Aldrich) as previously described (Walsh et al., 2010). HUVECs and HPAECs (Lonza) were propagated as previously described (Lawson et al., 2012) and used at passages <10. VEC-null ECs (Carmeliet et al., 1999) were obtained from E. Dejana. Murine ID8 ovarian carcinoma, ID8-IP, and human 293T cells were used as previously described (Tanjoni et al., 2010). ID8 expressing murine VEGF-A (ID8-VEGF) was created as previously described (Weis et al., 2004). RFP (pDsRed-Express-C1; Takara Bio Inc.) was subcloned into the lentiviral expression vector (pCDH-cytomegalovirus-MSC1; System Biosciences). Lentivirus-transduced DsRed-expressing B16F10 cells were selected (2 µg/ml puromycin), expanded, and frozen as low passage stocks. Lentivirus-transduced mCherry-expressing ID8-IP cells were puromycin selected.

Murine ECs
Primary mHLECs were isolated from tissue by magnetic bead anti-CD31 and anti-CD102 binding. Isolated ECs were verified for acetylated low density lipoprotein uptake and for CD31 and ICAM-2 surface expression by flow cytometry as previously described (Chen et al., 2012) and using the relevant antibodies described in Table S1. mHLECs were treated with adenoviral Cre to promote floxed FAK excision and used at passages <5 without immortalization. mHLECs were maintained in EBM-2 basal EC medium (Lonza) with microvascular supplementation (BulletKit; Lonza) and 10% FBS on plates coated with 0.2% gelatin and 10 µg/ml rat tail collagen I (EMD Millipore).

Antibodies and reagents
VEC pY658 antibody used for immunostaining was developed by E. Dejana (Orsenigo et al., 2012). PF-562271 (PF-271) was synthesized by Laviana Corporation as previously described (Roberts et al., 2008). The resulting material was 98% pure by HPLC with mass verified by MS and nuclear magnetic resonance (Laviana Corporation). PND-1186 was obtained from Poniard Pharmaceuticals. For cell culture, PF-271 and PND-1186 were dissolved in DMSO. Dasatinib was obtained from ChemieTek. Additional antibody and reagent information is provided in Table S1.

DNA constructs
Human VEC fused in frame to GFP in pCDNA3.1 was created as previously described (Potter et al., 2005). The VEC cytoplasmic domain (sequence coding for residues 621–784) was amplified by PCR and subcloned into pEBG for mammalian GST fusion protein expression or subcloned into pGEX-4T1 for bacterial GST fusion protein expression in BL21(DE3)pLysS (EMD Millipore) and purified using chromatography (Profinia; Bio-Rad Laboratories). Expression vectors containing VEC-Y658F, -Y685F, and -Y733F point mutations fused in frame to GFP were created as previously described (Turowski et al., 2008). Constructs were subcloned into pCDH-MCS1-EF1-puromycin (System Biosciences) for lentiviral expression and verified by sequencing. Lentiviral production and EC transduction was performed as previously described (Lawson et al., 2012). In brief, 293T cells

were cotransfected with pLentiLox3.7 or pCDH constructs in combination with envelope, reverse transcription, and viral packaging vectors. Lentivirus-containing media were harvested after 48 h, filtered, and used to infect ECs in the presence of 5 µg/ml polybrene for 2 d. VEC-GFP–reexpressing ECs were selected with 1 µg/ml puromycin and verified as GFP positive by flow cytometry (FACSCalibur; BD).

Signaling

Tamoxifen-treated FAK-WT and FAK-KD mice were tail vein injected with 0.2 mg/kg VEGF-A (in 100 µl PBS) or PBS alone, and after 2 min, hearts and lungs were rapidly excised and homogenized for 30 s using a tissue homogenizer (Precellys 24; Bertin Technologies) in cell lysis buffer (1% Triton X-100, 1% sodium deoxycholic acid, 0.1% SDS, 50 mM Hepes, pH 7.4, 150 mM NaCl, 10% glycerol, 1.5 mM MgCl$_2$, 1 mM EGTA, 10 mM sodium pyrophosphate, 100 mM NaF, 1 mM sodium orthovanadate, 10 µg/ml leupeptin, and 10 µg/ml aprotinin). Confluent HUVECs or mHLECs were starved for 2 h in EBM-2 basal EC medium (Lonza) without supplements before 50 ng/ml VEGF-A (10 min) addition. 1 µM PF-271 was added on HUVECs 1 h before VEGF-A treatment. For tumor cell–initiated signaling, 10^6 ID8 or ID8-VEGF tumor cells washed in PBS were added to a confluent monolayer of starved HUVECs ($\sim$5 × 10^6 cells) for 6 h in the presence of DMSO or 1 µM PF-271. Cells were washed in PBS, and proteins were extracted in cell lysis buffer and analyzed by SDS-PAGE and immunoblotting. For tumor cell–initiated in vivo signaling analyses, C57BL/6, FAK-WT, or FAK-KD mice were tail vein injected with 100 µl PBS, ID8, or ID8-VEGF (0.5 × 10^6 cells in 100 µl PBS), and lung extracts were analyzed after 6 h.

VEGF ELISA

Murine VEGF-A in the media from ID8, ID8-VEGF, ID8-IP, and B16F10 tumor cells after 48 h was quantified via ELISA (R&D Systems). Enumeration of viable cells was evaluated by automated trypan blue staining and counting (Vi-CELL XR; Beckman Coulter) from three chambers per experimental point and four independent experiments.

In vitro kinase assay

293T cells were transfected with pEBG VEC 621–784 or pEBG control using jetPRIME (Polyplus Transfection), protein lysates were made after 48 h, and GST fusion proteins were collected by glutathione–agarose bead (Sigma-Aldrich) binding. Beads were washed three times in cell lysis buffer and twice in kinase buffer (20 mM Tris HCl, pH 7.5, 200 mM NaCl, 0.5 mM Na$_3$VO$_4$, 25 mM MgCl$_2$, 5 mM MnCl$_2$, 1 mM EDTA, and 5 mM β-mercaptoethanol). Kinase assays were initiated by 200 µM ATP addition with 2 µg GST fusion protein, 250 ng of purified recombinant FAK domain, or 50 ng of purified full-length His-tagged c-Src from baculovirus (Wu et al., 2008) in the presence of 0.5 µM PF-271 or DMSO for 15 min at 32°C. Reactions were stopped by the addition of SDS sample buffer for immunoblotting. For MS, bacterial-purified GST-VEC 621–784 was used in the kinase assay, and reactions were stopped by freezing.

MS

Kinase reactions were thawed and diluted in 50 mM Tris, pH 8.0, 100 mM NaCl, and 1 mM EDTA with the addition of RapiGest SF (Waters Corp.) to 0.1% and boiled for 5 min. Tris 2-carboxyethyl phosphine was added to 1 mM, and samples were incubated at 37°C for 30 min and carboxy-methylated by 0.5 mg/ml iodoacetamide addition for 30 min at 37°C followed by 2 mM Tris 2-carboxyethyl phosphine neutralization. Samples were digested with GluC followed by trypsin (protease/protein ratio at 1:50) for 24 h. RapiGest was removed by treating with 250 mM HCl at 37°C for 1 h followed by centrifugation at 14,000 rpm for 30 min at 4°C. Peptides were extracted from the soluble fraction, desalted (Aspire RP20; Thermo Fisher Scientific), and separated by nanoscale high pressure liquid chromatography (Tempo; Applied Biosystems) using 10 cm–100 µm ID glass capillary packed column with 5-µm C18 beads (Zorbax; Agilent Technologies). Peptides were eluted using a linear acetonitrile gradient (5–60%) interfaced with tandem MS (liquid chromatography-MS/MS) using nanospray ionization and a hybrid mass spectrometer (TripleTOF 5600; AB SCIEX). MS/MS data were acquired in a data-dependent manner, whereby MS1 data were acquired for 250 ms at a mass/charge ratio of 400–1,250 D, and the MS/MS data were acquired from mass/charge of 50–2,000 D. For independent data acquisition parameters, MS1 time of fight was 250 ms followed by 25 MS2 events of 100 ms each. The independent data acquisition criteria were an over 300 counts threshold and a charge state of 2–4 with 4-s exclusion. MASCOT (Matrix Sciences) and ProteinPilot 4.0 (AB SCIEX) were used for peptide identifications and phosphorylation analysis.

Tumor models

ID8-IP orthotopic tumor growth was performed by surgical implantation of mCherry-labeled cells unilaterally under the ovarian bursa of 8–10-wk-old C57BL/6 mice as previously described (Ward et al., 2013). Oral gavage of 30 mg/kg PF-271 or vehicle was started at day 7 and maintained twice daily through termination (day 28). 4T1-L orthotopic breast tumor growth was performed by T4 mammary fat pad injection into 8–10-wk-old BALB/c mice as previously described (Walsh et al., 2010). Ad libitum, 0.5 mg/ml PND-1186 (in 5% sucrose) or vehicle was initiated at day 3 and maintained through termination (day 22). DsRed-B16F10 orthotopic melanoma tumor growth was performed by subcutaneous injection in the flank (10^6 cells in 100 µl PBS) or in the ear (0.5 × 10^6 cells in 6 µl growth factor–depleted Matrigel; BD) of FAK-WT or FAK-KD mice. Flank tumor volume was measured by microcalipers using the formula V = a × b^2/2 (a = length; b = width). Ears with B16F10 tumors were dissected at day 21, and DsRed-positive fluorescent primary tumor area was visualized using a small animal imaging system (OV100; Olympus) with an electron-multiplying charge-coupled device camera (ImagEM; Hamamatsu Photonics) and quantified using ImageJ (National Institutes of Health).

Immunostaining

Paraffin-embedded normal breast and late-stage breast cancer tissue array (BR8013; US Biomax) sections were deparaffinized, rehydrated, processed for antigen retrieval, and quenched for peroxidase activity. Sections were blocked (PBS, 1% BSA, and 0.1% Triton X-100) for 45 min at RT and incubated with anti-pY397 FAK (1:100) overnight followed by biotinylated goat anti–rabbit IgG (1:300) for 30 min, and antibody binding was visualized with diaminobenzidine and counterstained with hematoxylin (Vectastain ABC Elite; Vector Laboratories). Images were captured using an upright microscope (40× Plan Apochromat, NA 0.95; BX43; Olympus) and a color camera (SC100; Olympus). 7-µm frozen tumor and lung sections (CM1950; Leica) were fixed in cold acetone (10 min), rehydrated in PBS containing 0.5% BSA (5 min), and blocked (1.25% normal goat serum in PBS) for 30 min. Samples were incubated with anti-FAK pY397 (1:25) or anti-VEC pY658 (1:10) and anti-CD31 (1:300) overnight at 4°C in blocking buffer followed by Alexa Fluor 488 goat anti–rabbit (1:500) or Alexa Fluor 594 goat anti–rat (1:500) with DAPI (45 min) at RT. Confluent HPAEC cells, starved for 16 h, pretreated with 1 µM PF-271 or 100 nM Dasatinib were treated with 50 ng/ml VEGF-A (10 min) before fixation (3.7% paraformaldehyde for 10 min), permeabilization (0.2% Triton X-100 in PBS for 10 min), and blocking (2% BSA, 0.2% Triton X-100, and 0.05% Tween in PBS) for 1 h. Samples were incubated with FAK (1:50), pY416 c-Src (1:50), and VEC (1:25) or FAK (1:50) antibodies overnight at 4°C in blocking buffer followed by Alexa Fluor 488 goat anti–mouse, Alexa Fluor 488 goat anti–rabbit, Alexa Fluor 594 goat anti–mouse, or Alexa Fluor 594 goat anti–rabbit with DAPI (45 min) at RT. Images were acquired sequentially using a spinning-disk confocal microscope (IX81; Olympus) at 60× (Plan Apochromat, NA 1.42) and a charge-coupled device camera (ORCA-ER; Hamamatsu Photonics) controlled by SlideBook (v5.0) software (Intelligent Imaging Innovations). A mercury lamp source, multiband dichroic, single-band exciter, and single-band emitter filter sets (Chroma Technology Corp.) on dual filter wheels were used. Files were cropped, pseudocolored, and contrast adjusted using Photoshop (Adobe). Quantification was performed using ImageJ.

VEC internalization

VEC internalization analyses were performed as previously described (Gavard and Gutkind, 2006). In brief, confluent HPAECs were starved (16 h), pretreated with DMSO or 1 µM PF-271 at 37°C, and incubated with anti-VEC extracellular domain antibodies (BV6; 1:100) with or without PF-271 for 30 min on ice, and unbound antibody was removed by rinsing cells in ice-cold Hepes-containing EBM-2 media. HPAECs were treated with 50 ng/ml VEGF-A (with or without PF-271 for 30 min at 37°C), surface-bound antibody was removed by an acid wash (PBS, 25 mM glycine, pH 2.7, and 3% BSA) for 15 min, and HPAECs were fixed in 3.7% paraformaldehyde in PBS (10 min). HPAECs were permeabilized (0.2% Triton X-100 in PBS for 10 min) and incubated in blocking buffer (2% BSA in PBS) overnight, internalized anti-VEC was detected with Alexa Fluor 488 goat anti–mouse (1:500; 30 min at RT), and nuclei were stained with DAPI. Images were acquired and processed as described for Immunostaining.

Paracellular permeability

10^5 ECs were plated in Transwell chambers (6.5-mm diameter and 0.4-µm pore size; Costar), grown for 3 d, and serum starved for 4 h. HRP-conjugated IgG (4 µg/ml) and VEGF (100 ng/ml) were added to the upper chamber. After 15 min, 10 µl of media was removed from the lower chamber,

the amount of HRP-conjugated IgG was determined by ELISA (Ultra 3,3′,5,5′ tetramethylbenzidine; Thermo Fisher Scientific), and fluorescence was quantified (450-nm plate reader; Tecan). Mean values were obtained from three independent experiments performed in triplicate.

Adhesion and transmigration assays

0.25×10^6 HUVECs, mHLECs, or reconstituted VEC-null ECs were plated in 24-well dishes precoated with 0.1% gelatin plus 2% collagen in full media for 24 h. To measure tumor cell adhesion, 5-chloromethylfluorescein diacetate (CMFDA)- or DiIC12(3)-labeled ID8, ID8-VEGF, or B16F10 tumor cells (10^5) were added to EC monolayers at 37°C, and after 45 min, unbound cells were removed by PBS wash, and bound cells were visualized by confocal microscopy after paraformaldehyde fixation. To measure tumor cell transmigration, 10^5 ECs (HUVECs, FAK-WT mHLECs, FAK-KD mHLECs, and transfected VEC-null ECs) were grown until confluent in pre-coated (0.1% gelatin plus 2% collagen) HTS FluoroBlok inserts (8-µm pore size; Falcon; BD) and then starved in EBM-2 basal EC medium (Lonza) without supplements for 2 h. 10^4 CMFDA- or DiIC12(3)-prelabeled tumor cells were added to the top chamber in EBM-2 basal EC medium with 0.2% FBS and 2% FBS in the bottom chamber. At 3, 6, and 24 h, membrane underside images were obtained using a spinning-disk confocal microscope (IX81) at 10 or 20× (U Plan Fluor, NA 0.3; U Plan Apochromat, NA 0.75; Olympus). Cells per microscopic field were enumerated (nine fields per chamber) by thresholding using ImageJ. 1 µM PF-271 or DMSO was added 1 h before tumor cell addition where indicated. Mean values were obtained from three independent experiments of three chambers for each experimental point per assay.

Extravasation and metastasis

C57BL/6, FAK-WT, or FAK-KD mice at 10 wk of age were tail vein injected with DiIC12(3)-prelabeled B16F10, ID8, or ID8-VEGF (0.5 million in 100 µl PBS). At 6 or 16 h, blood vessels were labeled in situ by FITC-lectin injection. After 15 min, lungs were removed and sectioned using a razor blade, and whole-mount images (≥10 lung sections per mouse) were obtained using spinning-disk confocal microscope (IX81). In some experiments, whole-mount images were obtained using a laser-scanning confocal microscopy (Plan Apochromat 20×, NA 0.75; Eclipse C1si; Nikon) with EZ-C1 3.50 imaging software (Nikon). Tumor cell foci per field were enumerated using ImageJ. For experimental metastasis, cells were tail vein injected, and lungs were evaluated after 14 d. Tissue was fixed in Bouin's solution (Sigma-Aldrich), imaged with a digital camera, paraffin embedded, sectioned, and hematoxylin and eosin (H&E) stained. Lung metastases were enumerated by counting melanin-positive lesions in 10 sections spaced 50–100 µm apart per experimental point. Mean lung metastasis size was determined using ImageJ.

For spontaneous metastasis, 21 d after B16F10 ear injection, FAK-WT or FAK-KD mice were FITC-lectin injected (20 µg *Griffonia simplicifolia* agglutinin-I), and lungs were removed after 15 min, frozen, sectioned (10 µm; CM1950 cryostat), and analyzed by confocal microscopy. Images were sequentially acquired using a spinning-disk confocal microscope (IX81). Files were cropped, pseudocolored, and contrast adjusted using Photoshop. The mean number of lung micrometastases per field was determined by enumerating DsRed-positive lung lesions using ImageJ (v1.4) on ≥10 lung sections per mouse. Images were pseudocolored, overlaid, and merged using Photoshop.

Statistics

Differences between groups (one-way analysis of variance with Tukey's post hoc) and differences between pairs of data (unpaired two-tailed Student's *t* test) were analyzed using Prism (v5.0d; GraphPad Software), and values of <0.05 were considered significant.

Online supplemental material

Fig. S1 shows immunoblotting analyses of 4T1-L or ID8-IP tumor lysates, that ID8-IP cells implanted in the ovarian bursa region form distant metastasis, and selective VEC and VEGFR-2 expression in ECs but not in tumor cells. Fig. S2 provides a schematic of the inducible FAK-KD mouse model, a summary and heart lysate immunoblotting of in vivo VEGF signaling experiments, and a time course of VEGF-A– and TNF-stimulated signaling responses in HUVECs. Fig. S3 shows FAK-dependent β-catenin Y142 phosphorylation after ID8-VEGF adhesion to HUVECs and that FAK inhibition does not alter tumor cell adhesion to ECs. Fig. S4 shows that transfection of VEC-null ECs with Y to F VEC mutants does not impact VEGFR-2 activation or tumor cell adhesion to VEC-reconstituted ECs. Table S1 contains antibody and reagent information. Online supplemental material is available at http://www.jcb.org/cgi/content/full/jcb.201307067/DC1.

References

Abu-Ghazaleh, R., J. Kabir, H. Jia, M. Lobo, and I. Zachary. 2001. Src mediates stimulation by vascular endothelial growth factor of the phosphorylation of focal adhesion kinase at tyrosine 861, and migration and anti-apoptosis in endothelial cells. *Biochem. J.* 360:255–264. http://dx.doi.org/10.1042/0264-6021:3600255

Allingham, M.J., J.D. van Buul, and K. Burridge. 2007. ICAM-1-mediated, Src- and Pyk2-dependent vascular endothelial cadherin tyrosine phosphorylation is required for leukocyte transendothelial migration. *J. Immunol.* 179:4053–4064.

Arias-Pulido, H., N. Chaher, Y. Gong, C. Qualls, J. Vargas, and M. Royce. 2012. Tumor stromal vascular endothelial growth factor A is predictive of poor outcome in inflammatory breast cancer. *BMC Cancer.* 12:298. http://dx.doi.org/10.1186/1471-2407-12-298

Baumeister, U., R. Funke, K. Ebnet, H. Vorschmitt, S. Koch, and D. Vestweber. 2005. Association of Csk to VE-cadherin and inhibition of cell proliferation. *EMBO J.* 24:1686–1695. http://dx.doi.org/10.1038/sj.emboj.7600647

Bobek, V., K. Kolostova, D. Pinterova, G. Kacprzak, J. Adamiak, J. Kolodziej, M. Boubelik, M. Kubecova, and R.M. Hoffman. 2010. A clinically relevant, syngeneic model of spontaneous, highly metastatic B16 mouse melanoma. *Anticancer Res.* 30:4799–4803.

Carmeliet, P., M.G. Lampugnani, L. Moons, F. Breviario, V. Compernolle, F. Bono, G. Balconi, R. Spagnuolo, B. Oosthuyse, M. Dewerchin, et al. 1999. Targeted deficiency or cytosolic truncation of the VE-cadherin gene in mice impairs VEGF-mediated endothelial survival and angiogenesis. *Cell.* 98:147–157. http://dx.doi.org/10.1016/S0092-8674(00)81010-7

Chen, X.L., J.O. Nam, C. Jean, C. Lawson, C.T. Walsh, E. Goka, S.T. Lim, A. Tomar, I. Tancioni, S. Uryu, et al. 2012. VEGF-induced vascular permeability is mediated by FAK. *Dev. Cell.* 22:146–157. http://dx.doi.org/10.1016/j.devcel.2011.11.002

Chiang, A.C., and J. Massagué. 2008. Molecular basis of metastasis. *N. Engl. J. Med.* 359:2814–2823. http://dx.doi.org/10.1056/NEJMra0805239

Choi, C.H., B.A. Webb, M.S. Chimenti, M.P. Jacobson, and D.L. Barber. 2013. pH sensing by FAK-His58 regulates focal adhesion remodeling. *J. Cell Biol.* 202:849–859. http://dx.doi.org/10.1083/jcb.201302131

Claesson-Welsh, L., and M. Welsh. 2013. VEGFA and tumour angiogenesis. *J. Intern. Med.* 273:114–127. http://dx.doi.org/10.1111/joim.12019

Dejana, E., F. Orsenigo, and M.G. Lampugnani. 2008. The role of adherens junctions and VE-cadherin in the control of vascular permeability. *J. Cell Sci.* 121:2115–2122. http://dx.doi.org/10.1242/jcs.017897

Dejana, E., E. Tournier-Lasserve, and B.M. Weinstein. 2009. The control of vascular integrity by endothelial cell junctions: molecular basis and pathological implications. *Dev. Cell.* 16:209–221. http://dx.doi.org/10.1016/j.devcel.2009.01.004

Eccles, S.A., and D.R. Welch. 2007. Metastasis: recent discoveries and novel treatment strategies. *Lancet.* 369:1742–1757. http://dx.doi.org/10.1016/S0140-6736(07)60781-8

Gavard, J., and J.S. Gutkind. 2006. VEGF controls endothelial-cell permeability by promoting the beta-arrestin-dependent endocytosis of VE-cadherin. *Nat. Cell Biol.* 8:1223–1234. http://dx.doi.org/10.1038/ncb1486

Haskell, H., M. Natarajan, T.P. Hecker, Q. Ding, J. Stewart Jr., J.R. Grammer, and C.L. Gladson. 2003. Focal adhesion kinase is expressed in the angiogenic blood vessels of malignant astrocytic tumors in vivo and promotes capillary tube formation of brain microvascular endothelial cells. *Clin. Cancer Res.* 9:2157–2165.

Infante, J.R., D.R. Camidge, L.R. Mileshkin, E.X. Chen, R.J. Hicks, D. Rischin, H. Fingert, K.J. Pierce, H. Xu, W.G. Roberts, et al. 2012. Safety, pharmacokinetic, and pharmacodynamic phase I dose-escalation trial of PF-00562271, an inhibitor of focal adhesion kinase, in advanced solid tumors. *J. Clin. Oncol.* 30:1527–1533. http://dx.doi.org/10.1200/JCO.2011.38.9346

Labelle, M., and R.O. Hynes. 2012. The initial hours of metastasis: the importance of cooperative host-tumor cell interactions during hematogenous dissemination. *Cancer Discov.* 2:1091–1099. http://dx.doi.org/10.1158/2159-8290.CD-12-0329

Lawson, C., S.T. Lim, S. Uryu, X.L. Chen, D.A. Calderwood, and D.D. Schlaepfer. 2012. FAK promotes recruitment of talin to nascent adhesions to control cell motility. *J. Cell Biol.* 196:223–232. http://dx.doi.org/10.1083/jcb.201108078

Lee, J., A.K. Borboa, H.B. Chun, A. Baird, and B.P. Eliceiri. 2010. Conditional deletion of the focal adhesion kinase FAK alters remodeling of the bloodbrain barrier in glioma. *Cancer Res.* 70:10131–10140. http://dx.doi.org/10.1158/0008-5472.CAN-10-2740

Le Guelte, A., J. Dwyer, and J. Gavard. 2011. Jumping the barrier: VE-cadherin, VEGF and other angiogenic modifiers in cancer. *Biol. Cell.* 103:593–605. http://dx.doi.org/10.1042/BC20110069

Li, S., W. Dong, Y. Zong, W. Yin, G. Jin, Q. Hu, X. Huang, W. Jiang, and Z.C. Hua. 2007. Polyethylenimine-complexed plasmid particles targeting focal adhesion kinase function as melanoma tumor therapeutics. *Mol. Ther.* 15:515–523. http://dx.doi.org/10.1038/sj.mt.6300072

Liang, W., M. Kujawski, J. Wu, J. Lu, A. Herrmann, S. Loera, Y. Yen, F. Lee, H. Yu, W. Wen, and R. Jove. 2010. Antitumor activity of targeting SRC kinases in endothelial and myeloid cell compartments of the tumor microenvironment. *Clin. Cancer Res.* 16:924–935. http://dx.doi.org/10.1158/1078-0432.CCR-09-1486

Lietha, D., X. Cai, D.F. Ceccarelli, Y. Li, M.D. Schaller, and M.J. Eck. 2007. Structural basis for the autoinhibition of focal adhesion kinase. *Cell.* 129:1177–1187. http://dx.doi.org/10.1016/j.cell.2007.05.041

Lim, S.T. 2013. Nuclear FAK: a new mode of gene regulation from cellular adhesions. *Mol. Cells.* 36:1–6. http://dx.doi.org/10.1007/s10059-013-0139-1

Lim, S.T., X.L. Chen, A. Tomar, N.L. Miller, J. Yoo, and D.D. Schlaepfer. 2010. Knock-in mutation reveals an essential role for focal adhesion kinase activity in blood vessel morphogenesis and cell motility-polarity but not cell proliferation. *J. Biol. Chem.* 285:21526–21536. http://dx.doi.org/10.1074/jbc.M110.129999

Lim, S.T., N.L. Miller, X.L. Chen, I. Tancioni, C.T. Walsh, C. Lawson, S. Uryu, S.M. Weis, D.A. Cheresh, and D.D. Schlaepfer. 2012. Nuclear-localized focal adhesion kinase regulates inflammatory VCAM-1 expression. *J. Cell Biol.* 197:907–919. http://dx.doi.org/10.1083/jcb.201109067

Lu, C., T. Bonome, Y. Li, A.A. Kamat, L.Y. Han, R. Schmandt, R.L. Coleman, D.M. Gershenson, R.B. Jaffe, M.J. Birrer, and A.K. Sood. 2007. Gene alterations identified by expression profiling in tumor-associated endothelial cells from invasive ovarian carcinoma. *Cancer Res.* 67:1757–1768. http://dx.doi.org/10.1158/0008-5472.CAN-06-3700

Masoumi Moghaddam, S., A. Amini, D.L. Morris, and M.H. Pourgholami. 2012. Significance of vascular endothelial growth factor in growth and peritoneal dissemination of ovarian cancer. *Cancer Metastasis Rev.* 31:143–162. http://dx.doi.org/10.1007/s10555-011-9337-5

Mitra, S.K., S.T. Lim, A. Chi, and D.D. Schlaepfer. 2006. Intrinsic focal adhesion kinase activity controls orthotopic breast carcinoma metastasis via the regulation of urokinase plasminogen activator expression in a syngeneic tumor model. *Oncogene.* 25:4429–4440. http://dx.doi.org/10.1038/sj.onc.1209482

Obermayr, E., D.C. Castillo-Tong, D. Pils, P. Speiser, I. Braicu, T. Van Gorp, S. Mahner, J. Sehouli, I. Vergote, and R. Zeillinger. 2013. Molecular characterization of circulating tumor cells in patients with ovarian cancer improves their prognostic significance — a study of the OVCAD consortium. *Gynecol. Oncol.* 128:15–21. http://dx.doi.org/10.1016/j.ygyno.2012.09.021

Olsson, A.K., A. Dimberg, J. Kreuger, and L. Claesson-Welsh. 2006. VEGF receptor signalling - in control of vascular function. *Nat. Rev. Mol. Cell Biol.* 7:359–371. http://dx.doi.org/10.1038/nrm1911

Orsenigo, F., C. Giampietro, A. Ferrari, M. Corada, A. Galaup, S. Sigismund, G. Ristagno, L. Maddaluno, G.Y. Koh, D. Franco, et al. 2012. Phosphorylation of VE-cadherin is modulated by haemodynamic forces and contributes to the regulation of vascular permeability in vivo. *Nat Commun.* 3:1208. http://dx.doi.org/10.1038/ncomms2199

Palmer, S.R., L.A. Erickson, I. Ichetovkin, D.J. Knauer, and S.N. Markovic. 2011. Circulating serologic and molecular biomarkers in malignant melanoma. *Mayo Clin. Proc.* 86:981–990. http://dx.doi.org/10.4065/mcp.2011.0287

Poon, R.T., S.T. Fan, and J. Wong. 2001. Clinical implications of circulating angiogenic factors in cancer patients. *J. Clin. Oncol.* 19:1207–1225.

Potter, M.D., S. Barbero, and D.A. Cheresh. 2005. Tyrosine phosphorylation of VE-cadherin prevents binding of p120- and beta-catenin and maintains the cellular mesenchymal state. *J. Biol. Chem.* 280:31906–31912. http://dx.doi.org/10.1074/jbc.M505568200

Pylayeva, Y., K.M. Gillen, W. Gerald, H.E. Beggs, L.F. Reichardt, and F.G. Giancotti. 2009. Ras- and PI3K-dependent breast tumorigenesis in mice and humans requires focal adhesion kinase signaling. *J. Clin. Invest.* 119:252–266.

Roberts, W.G., E. Ung, P. Whalen, B. Cooper, C. Hulford, C. Autry, D. Richter, E. Emerson, J. Lin, J. Kath, et al. 2008. Antitumor activity and pharmacology of a selective focal adhesion kinase inhibitor, PF-562,271. *Cancer Res.* 68:1935–1944. http://dx.doi.org/10.1158/0008-5472.CAN-07-5155

Schulte, D., V. Küppers, N. Dartsch, A. Broermann, H. Li, A. Zarbock, O. Kamenyeva, F. Kiefer, A. Khandoga, S. Massberg, and D. Vestweber. 2011. Stabilizing the VE-cadherin-catenin complex blocks leukocyte extravasation and vascular permeability. *EMBO J.* 30:4157–4170. http://dx.doi.org/10.1038/emboj.2011.304

Schwock, J., N. Dhani, and D.W. Hedley. 2010. Targeting focal adhesion kinase signaling in tumor growth and metastasis. *Expert Opin. Ther. Targets.* 14:77–94. http://dx.doi.org/10.1517/14728220903460340

Shen, T.-L., A.Y.J. Park, A. Alcaraz, X. Peng, I. Jang, P. Koni, R.A. Flavell, H. Gu, and J.-L. Guan. 2005. Conditional knockout of focal adhesion kinase in endothelial cells reveals its role in angiogenesis and vascular development in late embryogenesis. *J. Cell Biol.* 169:941–952. http://dx.doi.org/10.1083/jcb.200411155

Steeg, P.S. 2006. Tumor metastasis: mechanistic insights and clinical challenges. *Nat. Med.* 12:895–904. http://dx.doi.org/10.1038/nm1469

Stokes, J.B., S.J. Adair, J.K. Slack-Davis, D.M. Walters, R.W. Tilghman, E.D. Hershey, B. Lowrey, K.S. Thomas, A.H. Bouton, R.F. Hwang, et al. 2011. Inhibition of focal adhesion kinase by PF-562,271 inhibits the growth and metastasis of pancreatic cancer concomitant with altering the tumor microenvironment. *Mol. Cancer Ther.* 10:2135–2145. http://dx.doi.org/10.1158/1535-7163.MCT-11-0261

Sun, Z., X. Li, S. Massena, S. Kutschera, N. Padhan, L. Gualandi, V. Sundvold-Gjerstad, K. Gustafsson, W.W. Choy, G. Zang, et al. 2012. VEGFR2 induces c-Src signaling and vascular permeability in vivo via the adaptor protein TSAd. *J. Exp. Med.* 209:1363–1377. http://dx.doi.org/10.1084/jem.20111343

Tanjoni, I., C. Walsh, S. Uryu, A. Tomar, J.O. Nam, A. Mielgo, S.T. Lim, C. Liang, M. Koenig, C. Sun, et al. 2010. PND-1186 FAK inhibitor selectively promotes tumor cell apoptosis in three-dimensional environments. *Cancer Biol. Ther.* 9:764–777. http://dx.doi.org/10.4161/cbt.9.10.11434

Tavora, B., S. Batista, L.E. Reynolds, S. Jadeja, S. Robinson, V. Kostourou, I. Hart, M. Fruttiger, M. Parsons, and K.M. Hodivala-Dilke. 2010. Endothelial FAK is required for tumour angiogenesis. *EMBO Mol Med.* 2:516–528. http://dx.doi.org/10.1002/emmm.201000106

Turowski, P., R. Martinelli, R. Crawford, D. Wateridge, A.P. Papageorgiou, M.G. Lampugnani, A.C. Gamp, D. Vestweber, P. Adamson, E. Dejana, and J. Greenwood. 2008. Phosphorylation of vascular endothelial cadherin controls lymphocyte emigration. *J. Cell Sci.* 121:29–37. http://dx.doi.org/10.1242/jcs.022681

Wallez, Y., F. Cand, F. Cruzalegui, C. Wernstedt, S. Souchelnytskyi, I. Vilgrain, and P. Huber. 2007. Src kinase phosphorylates vascular endothelialcadherin in response to vascular endothelial growth factor: identification of tyrosine 685 as the unique target site. *Oncogene.* 26:1067–1077. http://dx.doi.org/10.1038/sj.onc.1209855

Walsh, C., I. Tanjoni, S. Uryu, A. Tomar, J.O. Nam, H. Luo, A. Phillips, N. Patel, C. Kwok, G. McMahon, et al. 2010. Oral delivery of PND-1186 FAK inhibitor decreases tumor growth and spontaneous breast to lung metastasis in pre-clinical models. *Cancer Biol. Ther.* 9:778–790. http://dx.doi.org/10.4161/cbt.9.10.11433

Ward, K.K., I. Tancioni, C. Lawson, N.L. Miller, C. Jean, X.L. Chen, S. Uryu, J. Kim, D. Tarin, D.G. Stupack, et al. 2013. Inhibition of focal adhesion kinase (FAK) activity prevents anchorage-independent ovarian carcinoma cell growth and tumor progression. *Clin. Exp. Metastasis.* 30:579–594. http://dx.doi.org/10.1007/s10585-012-9562-5

Weis, S., J. Cui, L. Barnes, and D. Cheresh. 2004. Endothelial barrier disruption by VEGF-mediated Src activity potentiates tumor cell extravasation and metastasis. *J. Cell Biol.* 167:223–229. http://dx.doi.org/10.1083/jcb.200408130

Weis, S.M., S.T. Lim, K.M. Lutu-Fuga, L.A. Barnes, X.L. Chen, J.R. Göthert, T.L. Shen, J.L. Guan, D.D. Schlaepfer, and D.A. Cheresh. 2008. Compensatory role for Pyk2 during angiogenesis in adult mice

lacking endothelial cell FAK. *J. Cell Biol.* 181:43–50. http://dx.doi.org/
10.1083/jcb.200710038

Wu, L., J.A. Bernard-Trifilo, Y. Lim, S.T. Lim, S.K. Mitra, S. Uryu, M. Chen,
C.J. Pallen, N.K. Cheung, D. Mikolon, et al. 2008. Distinct FAK-Src ac-
tivation events promote alpha5beta1 and alpha4beta1 integrin-stimulated
neuroblastoma cell motility. *Oncogene*. 27:1439–1448. http://dx.doi.org/
10.1038/sj.onc.1210770

Zhao, X., X. Peng, S. Sun, A.Y. Park, and J.L. Guan. 2010. Role of kinase-
independent and -dependent functions of FAK in endothelial cell sur-
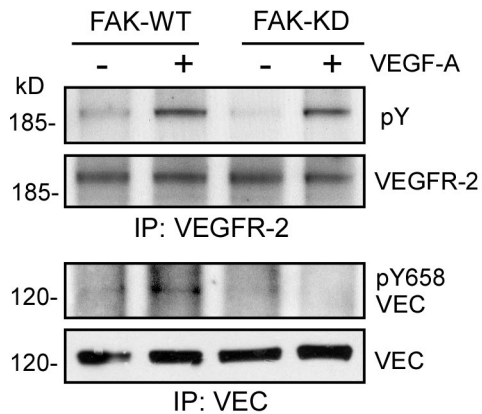vival and barrier function during embryonic development. *J. Cell Biol.*
189:955–965. http://dx.doi.org/10.1083/jcb.200912094

THE JOURNAL OF CELL BIOLOGY

Figure S1. **Effect of FAK inhibition in different tumor and cell models.** (A) Protein lysates from 4T1-L tumors implanted in the mammary fat pad (two independent controls and two treated with PND-1186) were analyzed for pY142 β-catenin and reprobed for β-catenin expression. (B) Fluorescently labeled ID8-IP tumor cells were surgically implanted in the ovarian bursa region of C57BL/6 mice. After 28 d, the ventral dermis was removed to expose the fluid-filled peritoneal cavity. The liver, lungs, kidneys, stomach, spleen, and intestine were surgically removed and photographed. Shown are representative images, and arrows point to local peritoneal and distant site ID8-IP metastatic tumor growth. (C) Lysates from FAK-WT and FAK-KD mouse heart and lung ECs (mHLEC), tumor cells (ID8, ID8-IP, and ID8-VEGF and B16F10), and human umbilical vein ECs (HUVEC) were evaluated for VEGFR-2, VEC, and actin expression by immunoblotting. (D) Densitometry of VEC pY658, total VEC, pY397 FAK, and total FAK in ID8-IP tumors from control and PF-271–treated mice from immunoblots shown in Fig. 1 D. Mean values are the ratio to actin levels ± SEM from three independent tumors (*, P < 0.05). Ratio from nontreated tumors was set at 100. (E) Immunoblotting of lysates from orthotopic ovarian ID8-IP tumors (three independent controls and three treated with PF-271) for pY142 β-catenin and pY416 c-Src and then reprobed for total β-catenin and c-Src. NT, not treated; WCL, whole-cell lysate.
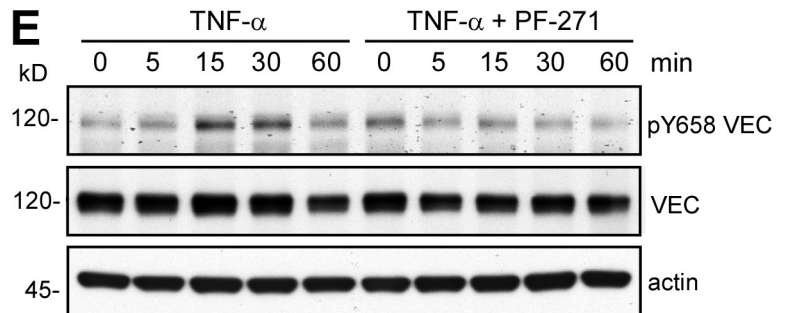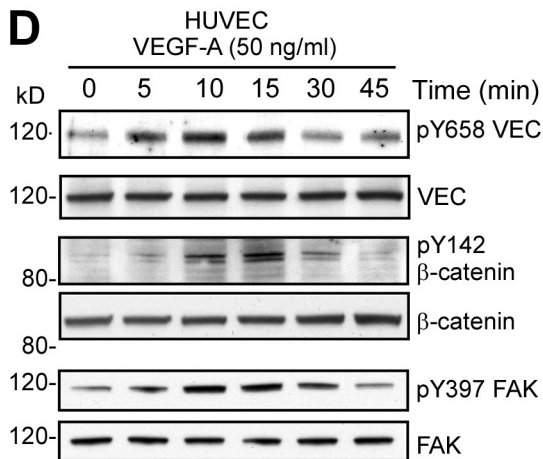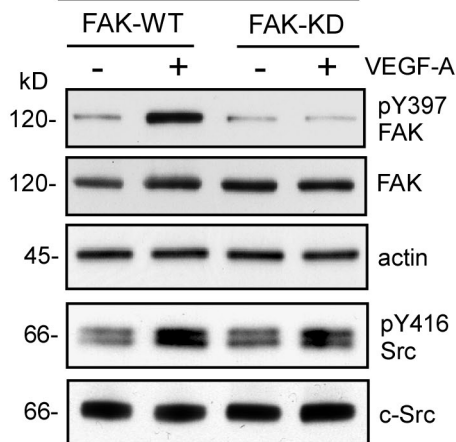
Figure S2. **VEGF-A stimulates VEC-Y658 phosphorylation in heart tissues and HUVEC cells.** (A) Progeny from FAK^{fl/fl} stem cell leukemia locus (SCL)–Cre-ER(T) and heterozygous FAK[KD/WT] crosses are treated with tamoxifen to induce Cre activation creating mice with hemizygous FAK-WT or FAK-KD expression in ECs. (B) Schematic of in vivo signaling assay using VEGF-A tail vein injection and rapid isolation of lung tissue. (C) Heart protein lysates from FAK-WT or FAK-KD mice tail vein injected with PBS or VEGF-A (0.2 mg/kg) were made within 2 min. Lysates were evaluated by VEGFR-2 immunoprecipitations (IP), phosphotyrosine (pY), and VEGFR-2 blotting. Lysates were analyzed by VEC pY658, FAK pY397, and c-Src pY416 phosphospecific immunoblotting and reprobed for total VEC, FAK, or c-Src. Actin was used as a loading control. (D) Confluent starved HUVECs were stimulated with 50 ng/ml VEGF-A for the indicated times, and lysates were analyzed for pY658 VEC, pY142 β-catenin, and pY397 FAK and then reprobed for total VEC, FAK, and c-Src. (E) Confluent starved HUVECs were pretreated or not treated with 1 µM PF-271 (60 min) and then stimulated with 10 ng/ml TNF for the indicated times. Lysates were analyzed for pY658 VEC, VEC, and actin by immunoblotting.
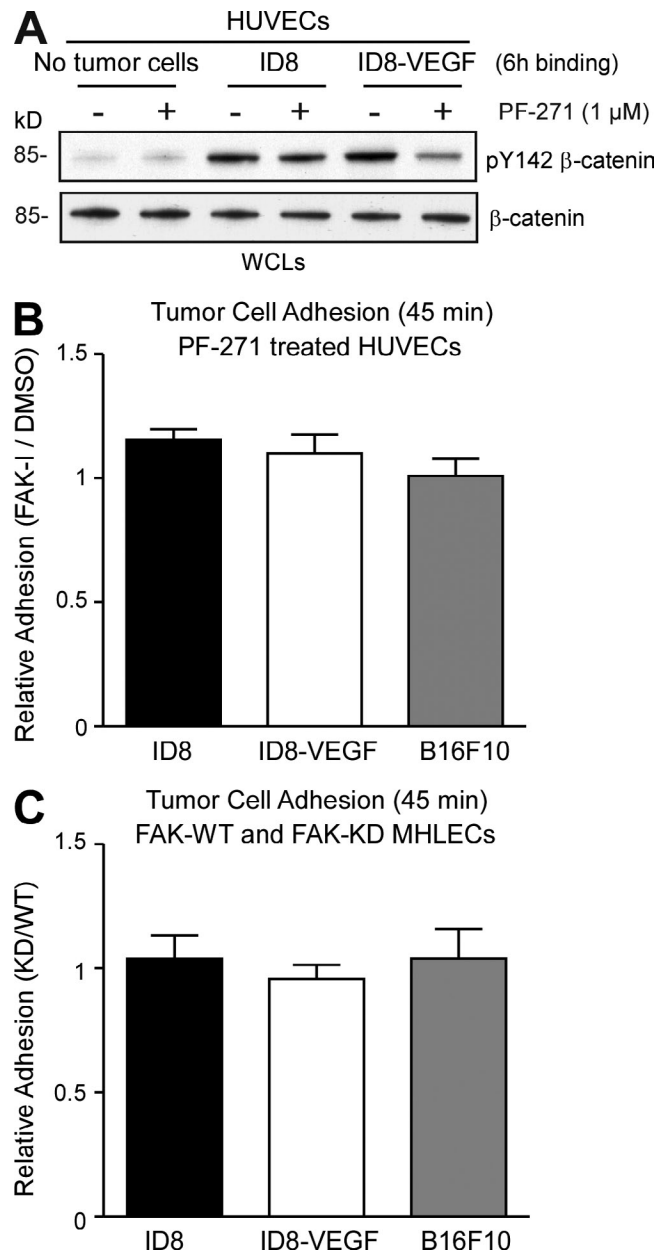
Figure S3. **Pharmacological or genetic EC FAK inhibition does not alter tumor-EC adhesion.** (A) No cell (control), ID8, or ID8-VEGF ovarian tumor cells were added to a HUVEC monolayer (1:5 tumor cell to HUVEC ratio) for 6 h in the presence of 1 µM PF-271 or DMSO as indicated. Whole-cell lysates (WCL) were analyzed by pY142 β-catenin and reprobed for total β-catenin. (B) The number of adherent fluorescently labeled ID8, ID8-VEGF, or B16F10 tumor cells to a HUVEC monolayer in the presence or absence of 1 µM PF-271 was determined at 45 min. (C) The number of adherent fluorescently labeled ID8, ID8-VEGF, or B16F10 tumor cells to a monolayer of FAK-WT or FAK-KD ECs was determined at 45 min. (B and C) Results are expressed as a ratio between PF-271/DMSO (B) or FAK-WT/FAK-KD (C) and are means ± SEM of three independent experiments.
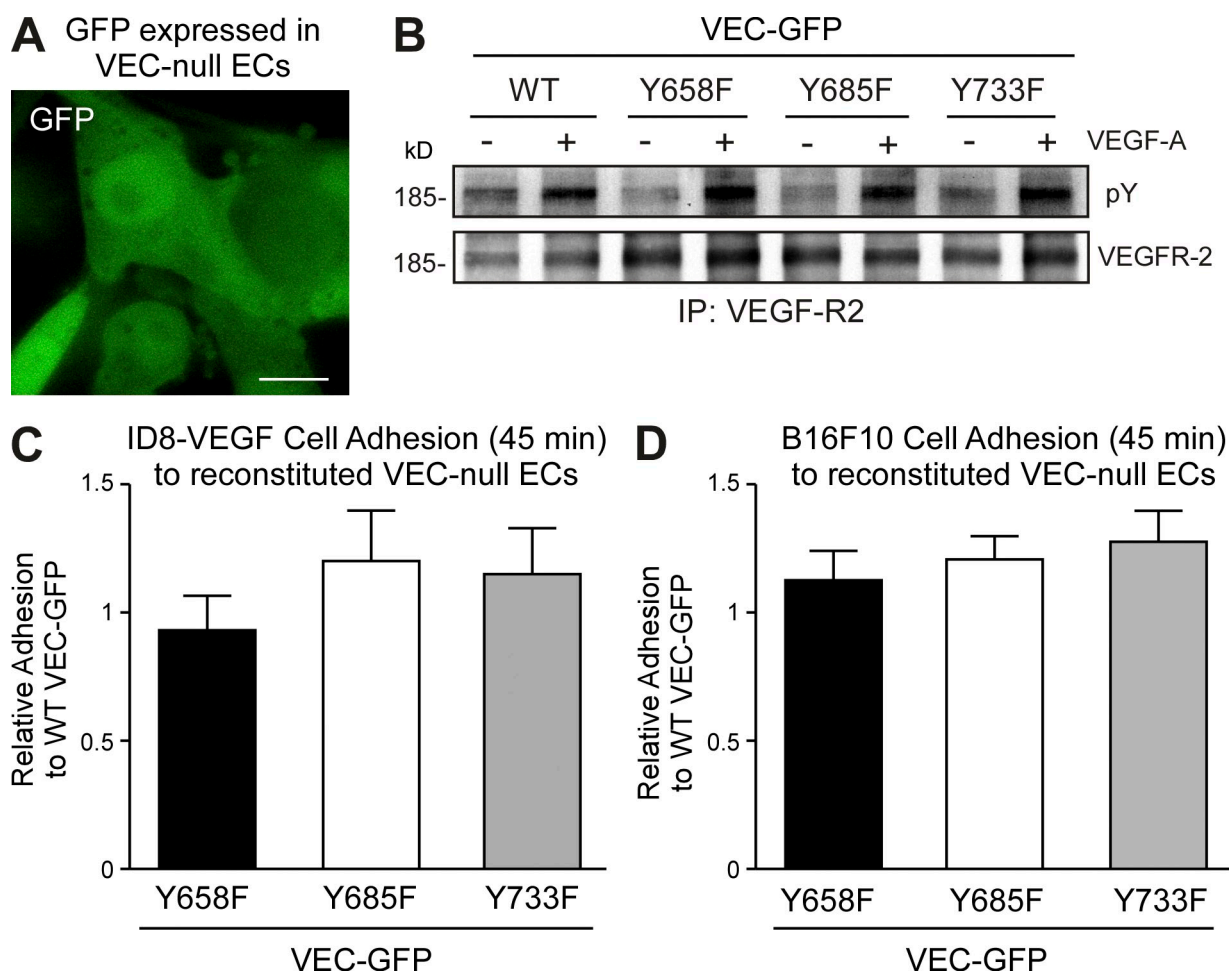
Figure S4. **VEC-GFP reexpression in VEC-null ECs does not alter VEGFR-2 activation or tumor–EC adhesion.** (A) Cytoplasmic localization of GFP in VEC-null ECs. Bar, 10 μm. (B) Equal activation of VEGFR-2 in VEC-null ECs expressing VEC-GFP WT or the indicated VEC-Y658F, -Y685F, or -Y733F point mutations. Cells were serum starved or stimulated with 50 ng/ml VEGF-A (10 min), and VEGFR-2 was isolated by immunoprecipitation (IP) and analyzed by antiphosphotyrosine (pY) immunoblotting. (C and D) The number of adherent fluorescently labeled ID8-VEGF (C) or B16F10 (D) tumor cells to a monolayer of VEC-null ECs expressing the indicated VEC-GFP constructs was determined at 45 min. Results are expressed as a ratio between WT and point mutant–expressing VEC-GFP cells and are means ± SD of three independent experiments.

Table S1.　**Antibodies and reagents used in this study**

Antibody/reagent	Reference/clone	Company
Anti–c-Src	sc-18	Santa Cruz Biotechnology, Inc.
Anti–VEGFR-2	sc-504	Santa Cruz Biotechnology, Inc.
Anti-VEC	Clones F8 and Z183	Santa Cruz Biotechnology, Inc.
Anti-VEC (for internalization)	Clone BV6	EMD Millipore
Anti-GAPDH	Clone 374	EMD Millipore
Anti-FAK	4.47	EMD Millipore
Anti–β-catenin	sc-7963	Santa Cruz Biotechnology, Inc.
Antiphosphotyrosine	4G10	EMD Millipore
Anti-VEC pY658 (immunoblotting)	AB1955	EMD Millipore
Anti-pY397 FAK	141-9	Life Technologies
Anti-pY397 FAK (immunohistochemistry)	ab4803	Abcam
Anti-pY142 β-catenin	ab83295	Abcam
Anti-pY416 c-Src	2101	Cell Signaling Technology
Anti-pY1175 VEGFR-2	19A10	Cell Signaling Technology
Anti–β-actin	AC-74	Sigma-Aldrich
Anti-GST	PI30001	Thermo Fisher Scientific
Anti-CD31	553370	BD
Anti–ICAM-2 (anti-CD102)	553326	BD
DilC12(3) fluorescent dye	354218	BD
CMFDA	C2925	Invitrogen
Goat anti–mouse Alexa Fluor 488	A-11001	Invitrogen
Goat anti–rabbit Alexa Fluor 488	A-11034	Invitrogen
Goat anti–rat Alexa Fluor 594	A-11007	Invitrogen
Goat anti–mouse Alexa Fluor 594	A-11005	Invitrogen
Goat anti–rabbit Alexa Fluor 594	A-11012	Invitrogen
Biotinylated goat anti–rabbit IgG	BA-1000	Vector Laboratories
VEGF-A	100-20	PeproTech
TNF	210-TA-020	R&D Systems